

# Outcrop-scale fracture systems in the Alpine foreland of central northern Switzerland: kinematics and tectonic context

Herfried Madritsch<sup>1</sup>

Received: 24 May 2015 / Accepted: 23 October 2015 / Published online: 25 November 2015  
© Swiss Geological Society 2015

**Abstract** This article summarizes the results of an extensive fieldwork-based analysis of outcrop-scale fractures across central northern Switzerland in the distal northern foreland of the Central Alps. The study focuses on the delineation of a relative fracture formation chronology, the fracture kinematics and their tectonic interpretation with the aim of enhancing the understanding of the study area's brittle deformation characteristics and history. The most commonly observed fractures within the analyzed outcrops of Middle and Upper Jurassic limestones are bedding-orthogonal joints, which show only minor increments of displacement (mode-II fractures). These structures formed relatively early during the tectonic evolution of the region and were repeatedly reactivated during later deformation events. Faults showing measurable displacements were observed comparatively rarely. Together with the results of fault-slip analyses, the outcrop-scale fracture patterns allow clear distinction of three major Cenozoic deformation steps in the study area: (1) formation of bedding-orthogonal joints lacking offsets and most likely related to regional uplift in Latest Mesozoic to Eocene times; (2) an only locally recognized phase of extension manifested by normal faults in the vicinity of the Hegau-Lake Constance Graben that onset after the Early Miocene; (3) shortening of the Alpine foreland from the Late Miocene onwards. Regionally recognizable NW–SE to NNW–SSE shortening, manifested by the strike-slip reactivation of bedding-orthogonal joints and normal faults, started

prior to the comparatively late formation of mapscale folds in the easternmost Jura Mountains but continued to be active throughout this deformation event. Only locally recognizable NNE–SSW to NE–SW directed shortening is also interpreted in the context of Late Miocene Alpine shortening and does not represent an independent regional stress field. The latter has apparently changed little from Late Miocene to recent times.

**Keywords** Fractures · Fault-slip analysis · Jura fold-and-thrust belt · Tabular Jura · Northern Switzerland

## 1 Introduction

The kinematic analysis of outcrop-scale fractures applying fault-slip analysis methods has a long tradition in central Western Europe and has proved to be a valuable approach to unravelling regional tectonic deformation histories (Plessmann 1972; Bergerat 1987; Larroque and Laurent 1988; Homberg et al. 2002; Sippel et al. 2009). The results of such analyses potentially allow local variations in deformation styles to be determined, insights gained into the role of fault reactivation and paleostress field reconstructions to be performed. This article summarizes the results of an extensive kinematic fault-slip analysis of such outcrop-scale fractures across central northern Switzerland in the northern Alpine foreland (Fig. 1). The aim of the field-based investigation was to decipher the multistage tectonic history of the region and provide a qualitative assessment of the intensity of deformation related to the various regionally recognized tectonic events. The investigation area has long been renowned for its excellent textbook outcrops of fracture systems (Ramsay and Huber 1987; Meier and Kronberg 1989; e.g. Fig. 2a). A thorough

---

Editorial handling: S. Schmid.

---

✉ Herfried Madritsch  
herfried.madritsch@nagra.ch

<sup>1</sup> Nagra, Hardstrasse 73, 5430 Wettingen, Switzerland

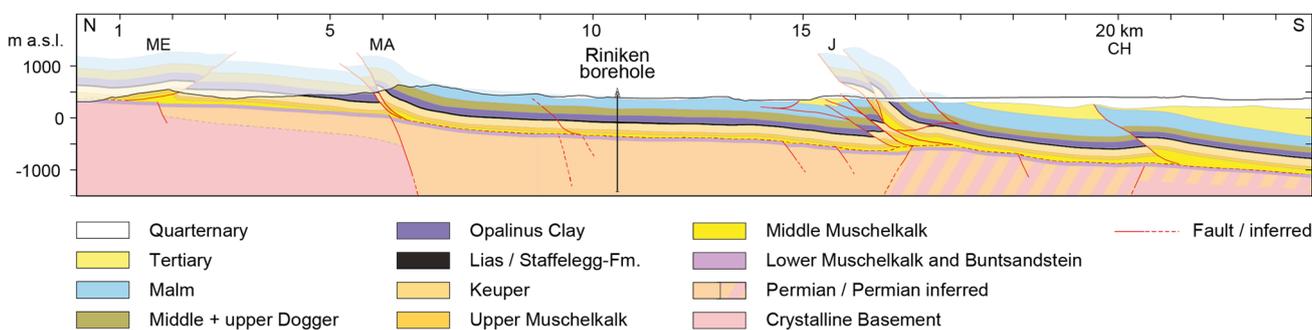
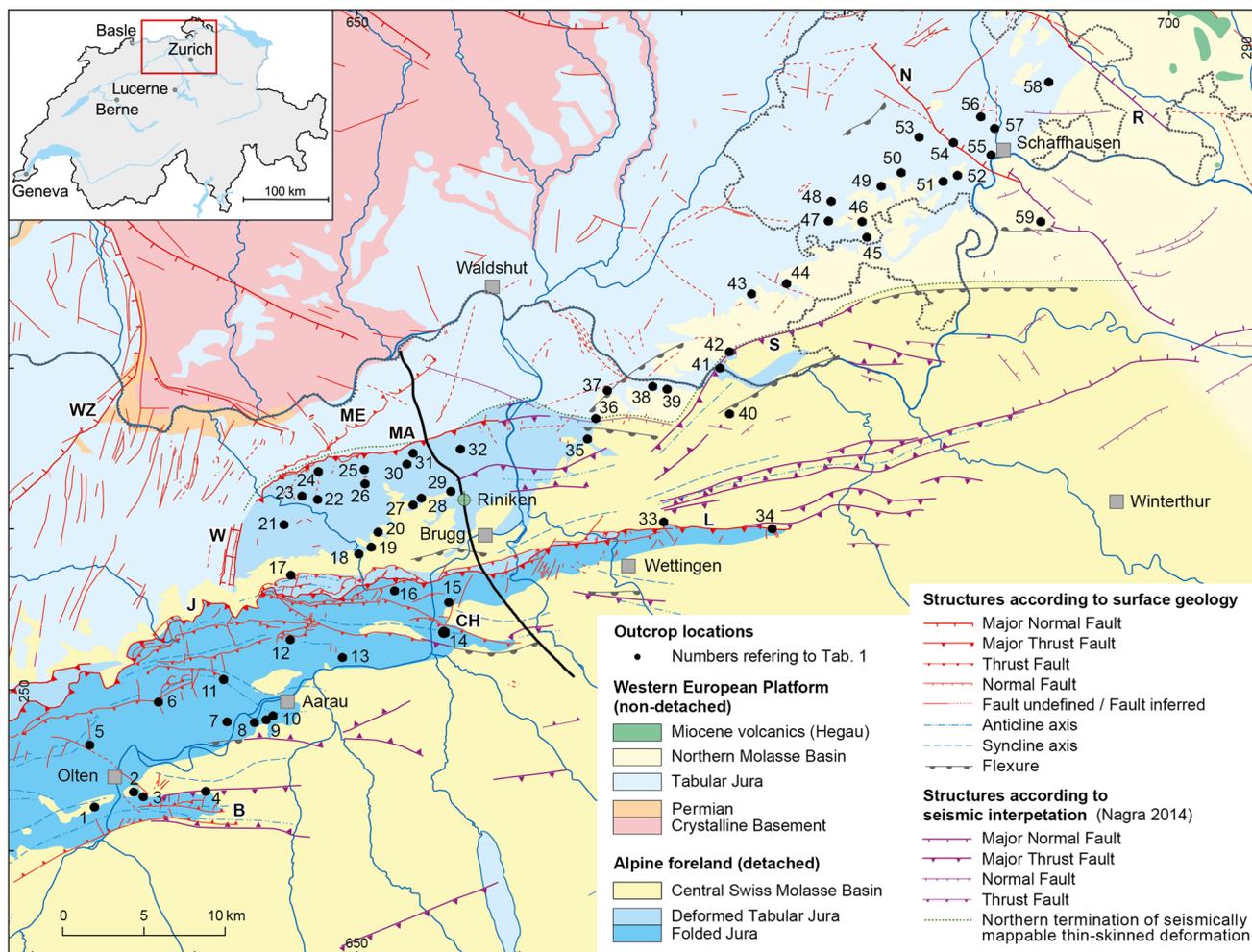


**Fig. 1** Tectonic map of the study area located in central northern Switzerland (modified after Nagra 2014). *Black dots* indicate the locations of outcrops where the fracture data discussed were collected. *Shades of blue* indicate the Folded Jura, Deformed Tabular Jura and Tabular Jura tectonic units (see text for discussion). The geological profile illustrates the general structure of the Jura Fold-

and-Thrust Belt. Selected regional fault zones mentioned in the text: *B* Born-Engelberg Anticline, *C* Chestenberg Thrust, *J* Jura Main Thrust, *L* Lägern Anticline, *MA* Mandach Thrust, *ME* Mettau Thrust, *N* Neuhausen Fault, *R* Randen Fault, *S* Siglistorf Anticline, *W* Wölflinswil Graben, *WZ* Wehra-Zeinigen Fault

understanding of the area’s brittle deformation history has become of particular interest as it is currently being considered for potentially hosting a future geological repository for radioactive waste and is being investigated

intensively on behalf of the Swiss National Cooperative for the Disposal of Radioactive Waste (Nagra). The article is based on a Nagra working report (Madritsch and Hammer 2012). It concentrates on the elaboration of a relative brittle

**Table 1** Characteristics of analyzed outcrops (compare Fig. 1) : XY: Swiss CH1903 coordinates; N: Number of relevant fracture measurements

Signature	Locality	X	Y	Lithology	Stratigraphic unit	Stratigraphic age	Tectonic unit	N
1	Born	633920	242490	Bedded, gently N-dipping limestone	Reuchenette Fm.	Malm	Folded Jura	30
2	Saeliwald	636330	243420	Bedded, gently N-dipping limestone	Villigen Fm.	Malm	Folded Jura	42
3	Oberwil	636920	243150	Well bedded, moderately N-dipping limestone	Villigen Fm.	Malm	Folded Jura	25
4	Daeniken	640760	243500	Bedded limestone	Villigen Fm.	Malm	Folded Jura	22
5	Trimbach	633640	246370	Well bedded, steeply S-dipping limestone	Hauptrogenstein Fm.	Dogger	Folded Jura	26
6	Reitflue	637870	249020	Well bedded, moderately S-dipping limestone	Hauptrogenstein Fm.	Dogger	Folded Jura	48
7	Niedergoesgen	642090	247800	bedded limestone	Wildegg Fm.	Malm	Folded Jura	27
8	Eppenber	643780	247760	Bedded limestone	Villigen Fm.	Malm	Folded Jura	33
9	Woeschnau	644530	247940	bedded limestone	Villigen Fm.	Malm	Folded Jura	44
10	Haseberg	644910	248160	Bedded limestone	Villigen Fm.	Malm	Folded Jura	38
11	Obererlinsbach	641870	250410	Well bedded, S-dipping limestone	Hauptrogenstein Fm.	Dogger	Folded Jura	30
12	Asperchus	646440	252920	S-dipping limestone	Hauptrogenstein Fm.	Dogger	Folded Jura	1
13	Biberstein	649210	251780	Bedded, gently S-dipping limestone	Wildegg Fm.	Malm	Folded Jura	18
14	Holderbank	655470	253320	Well bedded, S-dipping limestone	Wildegg Fm.	Malm	Folded Jura	34
15	Scherzberg	655760	255210	Bedded limestone	Villigen Fm.	Malm	Folded Jura	29
16	Heister	652410	255910	Bedded limestone	Hauptrogenstein Fm.	Dogger	Folded Jura	22
17	Densbueren	646020	256910	Well bedded, steeply S-dipping limestone	Hauptrogenstein Fm.	Dogger	Deformed Tabular Jura	34
18	Zeihen	650210	258210	Poorly bedded limestone	Wildegg Fm.	Malm	Deformed Tabular Jura	49
19	Saegimuhli	650980	258650	Bedded limestone	Villigen Fm.	Malm	Deformed Tabular Jura	41
20	Effingen	651400	259540	Bedded limestone	Villigen Fm.	Malm	Deformed Tabular Jura	37
21	Ueken	645600	260030	Well bedded limestone	Hauptrogenstein Fm.	Dogger	Deformed Tabular Jura	22
22	Hornussen	647660	261570	Bedded limestone	Hauptrogenstein Fm.	Dogger	Deformed Tabular Jura	23
23	Hammerei	646590	261960	Bedded limestone	Hauptrogenstein Fm.	Dogger	Deformed Tabular Jura	27
24	Itenthal	647700	263330	Bedded, moderately SE-dipping limestone	Hauptrogenstein Fm.	Dogger	Deformed Tabular Jura	27
25	Obersulz	650560	263460	Bedded limestone	Hauptrogenstein Fm.	Dogger	Deformed Tabular Jura	20
26	Elfingen	650600	262550	Well bedded limestone	Wildegg Fm.	Malm	Deformed Tabular Jura	13
27	Oberboezberg	653550	261240	Poorly bedded limestone	Villigen Fm.	Malm	Deformed Tabular Jura	67
28	Ueberthal	654080	261650	Well bedded limestone	Wildegg Fm.	Malm	Deformed Tabular Jura	27
29	Remigen	655890	262110	Bedded limestone	Wildegg Fm.	Malm	Deformed Tabular Jura	32
30	Moenthal	653160	263800	Well bedded, gently S-dipping limestone	Wildegg Fm.	Malm	Deformed Tabular Jura	39
31	Buererhorn	653560	264480	Well bedded, gently S-dipping limestone	Hauptrogenstein Fm.	Dogger	Deformed Tabular Jura	21
32	Gabenchofpf	656480	264720	Well bedded, gently S-dipping limestone	Villigen Fm.	Malm	Deformed Tabular Jura	42
33	Oberehrendingen	669000	260170	Steeply dipping, bedded limestone	Villigen Fm.	Malm	Folded Jura	24
34	Regensberg	675670	259780	Bedded limestone	Burghorn Fm.	Malm	Folded Jura	63
35	Endingen	664320	265360	Bedded limestone	Burghorn Fm.	Malm	Deformed Tabular Jura	33

Table 1 continued

Signature	Locality	X	Y	Lithology	Stratigraphic unit	Stratigraphic age	Tectonic unit	N
36	Untendingen	664820	266640	Bedded limestone	Villigen Fm.	Malm	Deformed Tabular Jura	55
37	Reckingen	665520	268350	Well bedded limestone	Wildeggen Fm.	Malm	Deformed Tabular Jura	63
38	Mellikon	668340	268610	Well bedded limestone	Villigen Fm.	Malm	Deformed Tabular Jura	41
39	Wislikofen	669230	268430	Well bedded limestone	Villigen Fm.	Malm	Deformed Tabular Jura	43
40	Fisibach-Tal	673050	267310	Bedded marls	Lower Freshwater Molasse	Miocene	Deformed Tabular Jura	–
41	Fisibach-Schlosswald	672470	269750	Bedded limestone	Villigen Fm.	Malm	Deformed Tabular Jura	32
42	Weilergraben	673040	270790	Bedded limestone	Burghorn Fm.	Malm	Deformed Tabular Jura	33
43	Netztal	674430	274350	Bedded limestone	Burghorn Fm.	Malm	Tabular Jura	41
44	Oberriedern	676590	275010	Bedded limestone	Villigen Fm.	Malm	Tabular Jura	13
45	Wangental	681510	277890	Bedded limestone	Plattenkalk Fm.	Malm	Tabular Jura	53
46	Rossherg	681210	278860	Bedded limestone	Wohlgessichichte Kalke Fm.	Malm	Tabular Jura	36
47	Wangental	679160	278890	Bedded limestone	Wohlgessichichte Kalke Fm.	Malm	Tabular Jura	26
48	Osterfingen	679330	280110	Bedded limestone	Wohlgessichichte Kalke Fm.	Malm	Tabular Jura	49
49	Tenggibuck	682430	281060	Well bedded limestone	Wohlgessichichte Kalke Fm.	Malm	Tabular Jura	49
50	Guntmadingen	683660	281900	Well bedded limestone	Wohlgessichichte Kalke Fm.	Malm	Tabular Jura	29
51	Brentenhau	686230	281350	Bedded limestone	Quaderkalk Fm.	Malm	Tabular Jura	42
52	Neuhuserwald	687100	281750	Bedded limestone	Plattenkalk Fm.	Malm	Tabular Jura	41
53	Loehningen	684750	284080	Bedded limestone	Wohlgessichichte Kalke Fm.	Malm	Tabular Jura	32
54	Beringen	686860	283760	Well bedded limestone	Wohlgessichichte Kalke Fm.	Malm	Tabular Jura	33
55	Schaffhausen	689170	282990	Bedded limestone	Plattenkalk Fm.	Malm	Tabular Jura	41
56	Holenbaum	688530	285360	Bedded limestone	Plattenkalk Fm.	Malm	Tabular Jura	23
57	Muehlental	689400	284640	Bedded limestone	Plattenkalk Fm.	Malm	Tabular Jura	42
58	Thayngen	692730	287530	Well bedded limestone	Plattenkalk Fm.	Malm	Tabular Jura	34
59	Benken	692430	279100	Sandstones and conglomerates	Upper Marine Molasse	Miocene	Swiss Molasse Basin	1

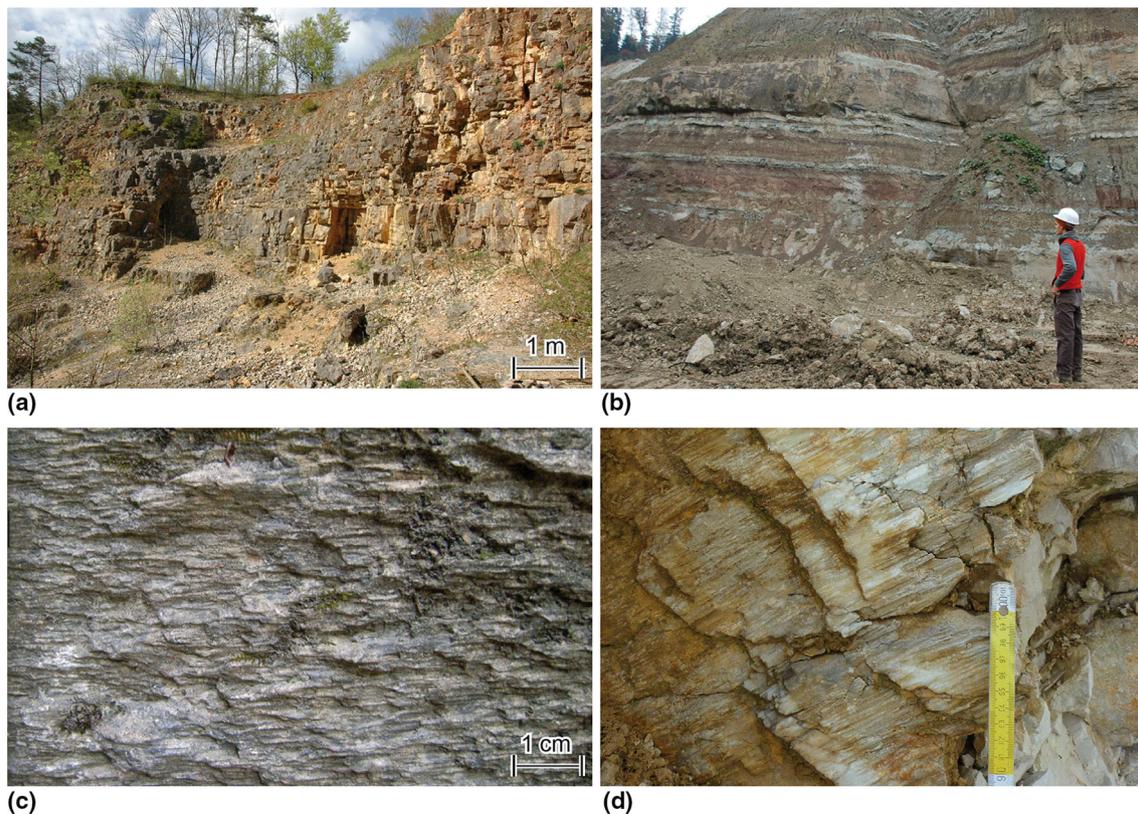


**Fig. 2** General field conditions and criteria for the kinematic analysis of outcrop-scale fracture systems in Northern Switzerland: **a** Late Jurassic limestones (here Villigen Fm.; outcrop 19) are typically characterized by closely spaced bedding-orthogonal fractures. **b** Hardly any fractures are observable in less competent marls and claystones (here: marls of the Lower Freshwater Molasse; USM;

outcrop 40). **c** Horizontal stylolite structures on a (in this case) vertical fracture plane. These so-called slickolites are the most common shear sense indicators observed in the study area (outcrop 9). **d** Slickenfibres that were comparatively rarely observed (outcrop 1). See Fig. 1 and in Table 1 for outcrop locations

deformation chronology for the region and its interpretation in the regional tectonic context.

## 2 Regional tectonic setting

The area of investigation is located in central northern Switzerland within the northern Alpine foreland (Fig. 1) and has witnessed a multistage tectonic history (e.g. Nagra 2014 and references therein). The Paleozoic basement, exposed in the adjacent Black Forest Massif is characterized by the Variscan orogeny (Thury et al. 1994). Post-orogenic extension and wrench faulting resulted in the formation of intramontane troughs during Carboniferous and Permian times. Major ductile shear and brittle deformation zones were formed with orientations typically being N–S, NW–SE and ENE–WSW. Several authors suggest multiple reactivations of these structures during Mesozoic and Cenozoic times (Laubscher 1970; Illies 1981; Ziegler 1992; Schumacher 2002; Wetzel et al. 2003; Ustaszewski et al. 2005; Madritsch et al. 2009). The most important

large-scale Pre-Mesozoic structure in the area of interest is the Permo-Carboniferous Trough of northern Switzerland (Diebold et al. 1991). The roughly ENE–WSW striking trough is completely buried by Mesozoic strata, but its geometry, with NW–SE and NNE–SSW striking faults as important segmenting elements, is quite well constrained from wells, seismic reflection and gravity data (see Nagra 2014 and references therein).

During the Mesozoic, the sedimentary sequence of the region evolved in an epicontinental marine environment (Geyer et al. 2011; Nagra 2014 and references therein). Successive periods of marine transgressions and regressions resulted in the deposition of terrestrial, evaporitic and shallow to deep marine sedimentary rocks (marls, claystones, limestones). This time period has long been considered to be characterized by relative tectonic quiescence (Naef et al. 1995). Several authors, however, have questioned this view and infer synsedimentary tectonic activity, based mainly on the observation of lateral sedimentary facies changes that seem to correlate with Paleozoic basement structures (e.g. Gygi 1986; Allenbach 2001; Wetzel et al. 2003).

The main structural units observable in the study area today result from its Cenozoic tectonic evolution. At the very end of the Mesozoic period the area of central northern Switzerland became affected by the far-field consequences of the Cretaceous Alpine orogeny that led to the closure of the Piedmont-Ligurian ocean (Pfiffner 1986; Schmid et al. 1996, 1997). Reconstructions of the Paleocene-Eocene northern coastline of the Alpine orogenic foredeep suggest that the area of investigation was located on top of a flexural forebulge zone whose formation led to uplift and erosion during Paleocene to Early Eocene times (Sinclair and Allen 1992; Kempf and Pfiffner 2004). The significant effect of this uplift in central northern Switzerland is demonstrated most clearly by a regionally recognizable erosional unconformity separating Late Jurassic limestones from Eocene residual clays (Müller et al. 2002). Fission track data from basement samples across the study area imply that a rapid cooling phase onset during the Late Cretaceous and continued into Paleogene times (Mazurek et al. 2006; Timar-Geng et al. 2006). Mazurek et al. (2006) estimated that 600–700 m of sediment was eroded, presumably including Cretaceous deposits that are not preserved in the study area today. The mode and extent to which the initiation and evolution of the lithospheric-scale forebulge structure has affected brittle deformation of the uppermost crust is poorly constrained.

The Eo-Oligocene formation of the European Cenozoic rift system led to the E–W to ESE–WNW directed opening of the Upper Rhine Graben located to the west of the study area (Laubscher 1970; Illies 1981; Ziegler 1992; Schumacher 2002; Hinsken et al. 2007). The small N–S striking Wölflinswil Graben (W in Fig. 1) forms the easternmost well-defined extensional structure that is presumably related to this rift system. The crystalline Black Forest Massif (Fig. 1) represents the eastern rift shoulder of the Upper Rhine Graben. Its exhumation was associated with normal faulting and took place during Late Oligocene to Early Miocene times (Ziegler 1992; Dèzes et al. 2004).

With the onset of the Cenozoic Alpine collision phase in Eocene times, the Alpine forebulge migrated northwards (Pfiffner 1986; Schmid et al. 1996, 1997; Kempf and Pfiffner 2004). The area of central northern Switzerland became submerged again and formed part of the northern Alpine Molasse Basin which developed in close response to syn- and post-collisional thrusting and erosion processes (Pfiffner 1986; Sinclair and Allen 1992; Schlunegger et al. 1997; Willet and Schlunegger 2010). Analyses of seismic reflection data across the study area suggest that this development also involved the reactivation of pre-existing basement faults related to the Permo-Carboniferous Trough of northern Switzerland (Diebold et al. 1991; Naef et al. 1995).

In the northeastern corner of the study area the Neuhausen and Randen Fault (N and R in Fig. 1 respectively) mark the westernmost bounding faults of the roughly NW–SE striking Hegau-Lake Constance Graben, a crustal-scale structure associated with the volcanic fields of the Hegau region (Ibele 2015 and references therein). The main phase of extensional deformation in the Hegau-Lake Constance Graben is reported to postdate Early Miocene times (Burdigalian; Hofmann et al. 2000; Schreiner 1992). Also the youngest preserved Molasse deposits (approximately 10 Ma according to Rahn and Selbekk 2007) are affected by normal faulting. Therefore, extensional to transtensional deformation in this area lasted until at least Late Miocene times and is probably still active today (Schreiner 1992; Naef et al. 1995; Müller et al. 2002; Ibele 2015 and references therein). The tectonic process responsible for this deformation is not fully understood; some authors infer a kinematic relation with the seismically active Albstadt shear zone of Western Germany (e.g. Reicherter et al. 2008).

Also around the Late Miocene, the Alpine deformation front propagated far into the northern foreland along a décollement horizon in Middle to Late Triassic evaporites (e.g. Laubscher 1972; Burkhard 1990; Jordan et al. 1990; Jordan 1992). At the northern edge of the central Swiss Molasse Basin, this process resulted in the formation of the Jura mountain range that is widely accepted as representing a thin-skinned foreland fold-and-thrust belt (Laubscher 1972; Sommaruga 1997). The easternmost tip of the Jura range dissects the study area from east to west (Fig. 1). The main deformation zone is commonly referred to as the Folded Jura (Fig. 1) and is characterized by closely spaced thrusts and tight thrust-related folds (Buxtorf 1907; Laubscher 1986; Diebold and Noack 1997; Malz et al. 2015). The predominantly ENE–WSW striking folds and thrusts are occasionally cut by N–S and NW–SE striking faults. The Jura Main Thrust (J in Fig. 1) forms the boundary between the Folded Jura and a northward adjacent zone, characterized by much less but still traceable contractional deformation. This so-called “Vorfalltzone” (Nagra 2014) is referred to herein as the Deformed Tabular Jura (Fig. 1). It must be regarded as part of the Jura Fold-and-Thrust Belt, due to the occurrence of décollement-related thrusts defining its northern boundary. In the west of the study area, this boundary is formed by the prominent Mandach Thrust (MA in Fig. 1; Laubscher 1986) which crops out at the surface, whereas towards the east it is represented by the Siglistorf Thrust (S in Fig. 1) that has only been revealed through reflection seismic investigations (e.g. Diebold et al. 1991; Naef et al. 1995). These thrusts form the northern termination of the seismically mapped area affected by thin-skinned deformation. The tectonic unit north of this deformation boundary is largely composed of Mesozoic sediments and is commonly referred to as the

Tabular Jura. With the exception of the Mettau Thrust (ME in Fig. 1; Wildi 1975), it does not feature regional-scale compressive structures. The Tabular Jura is therefore considered to rest autochthonously on the basement and not to be detached along the Triassic décollement horizon.

The main deformation phase of the Jura fold-and-thrust belt is considered to be a short-lived event that presumably lasted only until the Early Pliocene (e.g. Becker 2000). However, several geomorphological investigations at the front of the fold-and-thrust belt have revealed post-Pliocene activity (e.g. Nivière and Winter 2000; Giamboni et al. 2004; Madritsch et al. 2010). Based on geodynamic considerations, it was suggested that this most recent deformation is more likely due to thick-skinned foreland deformation rather than pure thin-skinned deformation (e.g. Mosar 1999). Indeed, interpretations of seismic reflection data west of Basel imply a component of thick-skinned deformation from the Late Pliocene onwards (Ustaszewski and Schmid 2007; Madritsch et al. 2008). Concerning recent tectonic activity, there are very few seismological indications for ongoing foreland compression in a thin-skinned and/or thick-skinned mode currently restricted to eastern France (Madritsch et al. 2008 with references therein). For the area of investigation, the instrumentally recorded moderate seismicity suggests a present-day tectonic regime of strike-slip to normal faulting (Kastrup et al. 2004).

### 3 Methodology

#### 3.1 Field mapping and kinematic interpretation

Careful field work is the key factor in a successful fault-slip analysis of outcrop-scale fracture systems (Sperner and Zweigel 2010; Hippolyte et al. 2012; Lacombe 2012). Acquisition locations have to be chosen with care to avoid selective sampling of orientation data and block rotations. The field interpretation of overprint criteria (e.g. superposed slickenfibres) needs to be particularly cautious as it is considered for the later separation of the fracture data into kinematically homogeneous subsets.

Competent rocks such as Middle Triassic, Middle and Upper Jurassic limestones (Fig. 2a) preferentially record brittle deformation in the study area (Meier and Kronberg 1989; Hergert et al. 2015) and are well suited for fault-slip analysis. In order to prevent an observational bias, mapping sectors were carefully chosen to include different rock face orientations in every outcrop (cf. Sperner and Zweigel 2010). In a first step, the mapped fractures were classified according to the two-fold classification of brittle deformation features (cf. Ramsay and Huber 1987): (1) faults that reveal a measurable amount of displacement, and (2)

faults that show no such displacement. As outlined in the results sections, this basic classification was further extended in order to better fit the actual structural features observable in the field area.

A major focus during field work was the identification of fault-slip indicators on the fracture planes, such as calcite growth fibres or slickolites that form by pressure solution (Fig. 2b, c; Hancock 1985; Petit 1987; Hippolyte et al. 2012). Wherever possible, the above-mentioned slip indicators were used to determine the shear sense along the fractures. The shear sense criteria were given quality marks ranging from 1 (excellent) to 3 (uncertain).

Besides the actual mapping of the deformation structures, a key factor for the later fault-slip analysis was the recognition of relative deformation chronologies in each analyzed outcrop. Several field criteria can be considered to establish such chronologies. Cross-cutting relationships are most reliable if an offset relationship between fracture sets that are not kinematically linked to each other (e.g. non-conjugated sets) is observable (Fig. 3). Overprinting

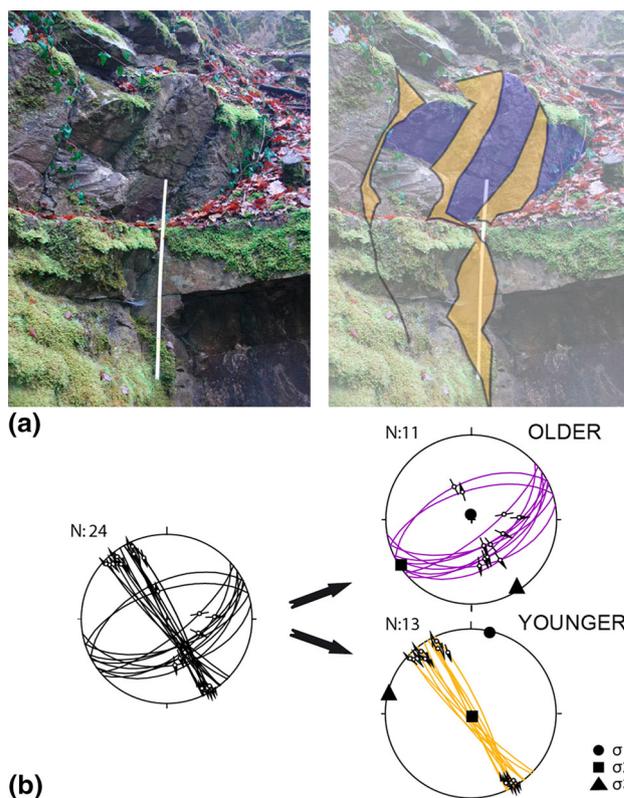


**Fig. 3** Example of field criteria used to establish relative deformation chronologies and separate fracture data into kinematically homogeneous subsets. **a** Cross-cutting relationship between two fracture sets within an outcrop of Upper Malm limestone (Plattenkalk Fm.; outcrop 51, see Fig. 1; Table 1 for location). A normal fault plane is cross-cut and slightly offset by vertical strike-slip faults and therefore regarded as being relatively older. **b** Illustration of the separation of the fracture dataset into two kinematically homogeneous subsets. Fracture data are illustrated as lower hemisphere equal area projections

relationships between different shear sense indicators on the same fault plane are also very commonly considered (Sperner and Zweigel 2010; Hippolyte et al. 2012). Meier and Kronberg (1989) suggested that fracture termination relationships can also point to relative chronologies, with older, pre-existing fractures preventing the propagation of relatively younger fracture sets. A very valuable criterion for establishing relative brittle deformation chronologies is based on the analysis of stress axis orientations derived from fault-slip data in tilted and folded terrain (Homberg et al. 1999). Stresses within the upper crust are considered to fulfil the Andersonian principle (Anderson 1942) that predicts two horizontally and one vertically oriented principal stress axes. If this principle is not fulfilled by a paleostress tensor derived by fault-slip analysis, the associated fault set has most likely been tilted/folded after its formation (provided it formed near the earth's surface). In such cases, none of the principal stress axes are vertical and two axes lie within the inclined bedding plane. Rotated fault-slip datasets and related paleostress axes fulfil the Andersonian model after back-tilting along the strike of the bedding plane by the amount of bedding dip. This criterion has already proved useful for distinguishing between pre-folding and post-folding fault-slip events along outcrop-scale fractures during similar studies within and around the Jura Fold-and-Thrust Belt (Homberg et al. 1999, 2002; Madritsch et al. 2008).

The TectonicsFP software package (Ortner et al. 2002) was used to process and evaluate the collected field data. Prior to fault-slip analysis, the field data gathered for each outcrop were separated into kinematically homogeneous fault-slip pair datasets. Where no direct field criteria for the fracture data separation were available, two separate graphical methods were applied to test the fault sets for kinematic homogeneity. The P–T axis method (Turner 1953; Marrett and Allmendinger 1990) is a kinematic fault-slip analysis technique based on the geometric construction of theoretical maximum, intermediate and minimum incremental strain axes which are calculated for each fault-slip pair. For kinematically homogeneous fault-slip datasets, the P and T axes usually form well defined clusters or systematic radial or axial distributions (Meschede 1994). In addition to this approach, tangent lineation projections of the fault-slip pairs (Hoepfner 1955; Meschede and Decker 1993; Sperner and Zweigel 2010) were considered as a second graphical method. In these projections, kinematically consistent fault-slip pairs are oriented towards or away from a common point in the projection plane which yields the position of the P and T axis respectively.

### 3.2 Fault-slip analysis

Two different basic hypotheses underlying fault-slip analysis can be distinguished (Twiss and Unruh 1998; Lacombe 2012). The first hypothesis assumes that the slip direction on a fault plane is parallel to the maximum resolved shear strain rate governed by a large-scale homogeneous strain rate tensor. The results of such a “kinematic analysis” yield the orientation of the principal axis of incremental strain based on the graphical or numerical construction of “kinematic axes”, or P–T axes, for each fault-slip pair (Marrett and Allmendinger 1990; Twiss and Unruh 1998). By contrast, the second hypothesis, also referred to as “dynamic analysis”, assumes that the slip direction on a fault plane is parallel to the direction of maximum resolved shear stress induced by a large-scale homogeneous stress field (Wallace 1951; Bott 1959; Angelier 1990). The results of a dynamic analysis give the orientation of the principal axes of stress ( $\sigma_1 > \sigma_2 > \sigma_3$ ) defining the paleostress tensor and represent a genetic interpretation of the observed structures (Marrett and Peacock 1999). Among several different types of dynamic analysis, fault-slip inversion is the one most commonly applied (Angelier 1990; Célérier et al. 2012).

Fault-slip analysis using inversion methods relies on several fundamental assumptions (see review in Lacombe 2012). Most importantly, it is presumed that the analyzed rock is physically and mechanically isotropic and behaves as a rheologically linear material (Twiss and Unruh 1998). Therefore, fault orientation in rocks should be random and different faults should not interact kinematically with each other; a theoretical requirement considered by an increasing number of authors to be hardly ever strictly fulfilled in nature (Pollard et al. 1993; Kaven et al. 2011). Despite the controversies concerning the actual geomechanical implications of fault-slip analysis, it is still considered to be a valuable method whose results have the potential to provide important insights into the evolution of regional deformation patterns, provided that data acquisition, separation and processing are carefully done and the results are interpreted with caution (Sperner and Zweigel 2010).

During this study, fault-slip analysis was carried out applying the Right-Dihedra method (Angelier and Mechler 1977; Pfiffner and Burkhard 1987) as featured by the TectonicsFP software package (Ortner et al. 2002). The Right-Dihedra method is considered to be a simple but robust dynamic fault-slip analysis approach (Angelier 1989). It delivers an estimation of the possible orientations of the principal stress axes ( $\sigma_1 > \sigma_2 > \sigma_3$ ), with the most likely orientation computed at point maxima of

superimposed compressional and tensional dihedra, calculated for each fault-slip pair (Angelier and Mechler 1977; Pfiffner and Burkhard 1987). Therefore, the Right-Dihedra method also considers movements along a non-random set of pre-existing fault planes that are not necessarily oriented ideally in terms of a theoretical best fit reduced stress tensor and may or may not be reactivated. In tectonic settings like the one of the study area, presumably characterized by polyphase brittle deformation, the Right-Dihedra method has proved to be particularly valuable since it was found to be less sensitive to highly asymmetric fault plane associations compared with other techniques (Meschede and Decker 1993).

A disadvantage of the Right-Dihedra method is that it does not directly yield the stress ratio ( $R = (\sigma_2 - \sigma_3) / (\sigma_1 - \sigma_3)$ ) allowing the tectonic regime in a given area to be described. This was acceptable given the rather simple fracture kinematics observed in the field where, in most cases, only the regimes of extension ( $\sigma_1$  vertical,  $\sigma_3$  horizontal), compression ( $\sigma_1$  horizontal,  $\sigma_3$  vertical) and strike-slip ( $\sigma_1$  and  $\sigma_3$  horizontal) needed to be distinguished. The results of the P–T axis method applied earlier to test the fault-slip datasets for kinematic homogeneity (see Sect. 3.1) were also considered in this regard and allowed defining the intermediate tectonic regime of transpression ( $\sigma_1$  horizontal,  $\sigma_3$  vertical to horizontal) and a great circle distribution of T-axis; Meschede 1994).

## 4 Results

### 4.1 Overview and general observations

In the course of this investigation, more than 200 outcrops within the study area were visited and 95 studied in detail (see also Madritsch and Hammer 2012). In this article, a selection of the most relevant outcrops for kinematic fracture analyses is presented and discussed, in particular those that yielded reliable information regarding the relative deformation chronology.

Limestones of Upper Jurassic age, in particular those of the Wildeggen and the Villigen Formations (Fig. 2a) together with those of the Middle Jurassic (Hauptrogenstein Formation), proved to be best suited for the fault-slip analyses. Outcrops of other Mesozoic and particularly Cenozoic rock formations, consisting predominantly of rheologically weak clastics (marls, clay- and sandstones; e.g. Fig. 2b), turned out to be poorly suited for the investigation purpose as they revealed little to no valuable information on brittle deformation. As a consequence of this field situation, the data gathered on brittle deformation only cover the Latest Mesozoic and Cenozoic tectonic history of the study area. Conclusions on deformation chronology during that time

have to rely mostly on relative cross-cutting/overprinting and not on stratigraphic criteria.

The dominant brittle deformation structures found in outcrops across the entire study area are bedding-orthogonal fractures (Figs. 2a, 4a). The normal spacing of these fractures is often very close (less than 1 meter) and increases with increasing bedding thickness (Meier and Kronberg 1989). The bedding orthogonal fractures hardly ever show significant offsets and are therefore to be classified as joints (Ramsay and Huber 1987). Close analyses of the joint planes allowed them to be divided from a mechanical perspective into mode-I and mode-II fractures. Mode-I/opening-type fractures that revealed no slip indications at all were not considered during the fault-slip analyses, in particular since their formation and, consequently, their tectonic significance is questionable for many



(a)



(b)

**Fig. 4** Field impressions of widely observed mode-I/mode-II type fractures. **a** Sub-vertical fractures orientated orthogonal to the bedding and cutting through an outcrop of Upper Malm limestone (Plattenkalk Fm.; outcrop 51). **b** Close-up view of a bedding-orthogonal fracture in thin bedded limestones of the Lower Malm Wildeggen Fm. (outcrop 30). The original mode-I fracture was filled with syntaxial calcite and later developed into a mode-II type fracture as evidenced by horizontal striations indicating strike-slip movement. See Fig. 1 and in Table 1 for outcrop locations

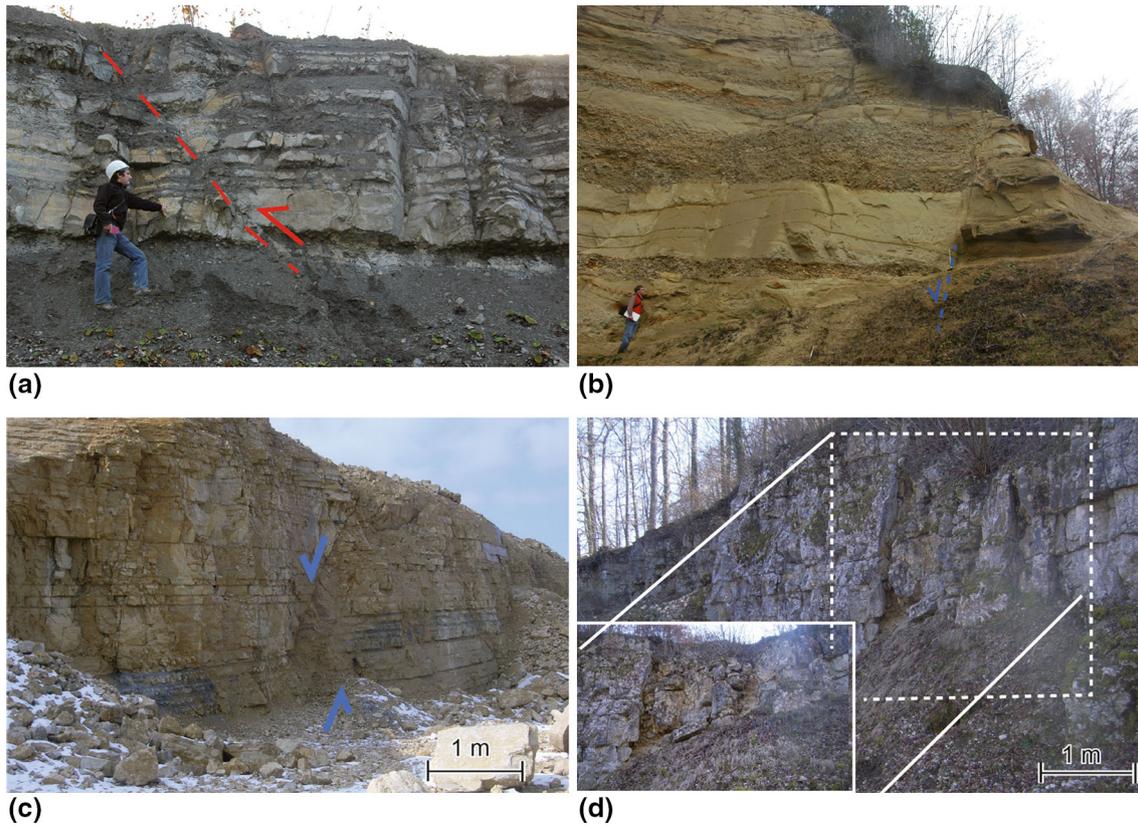


**Fig. 5** Field impressions of outcrop-scale faults as observable in the study area. **a** A reverse fault in thin bedded limestones and marls of the Lower Malm Wildegg Fm. (outcrop 37). **b** A normal fault cutting through clastic sediments of the Upper Marine Molasse showing several meters of vertical offset (outcrop 59). **c** A normal fault

offsetting bedded Upper Malm limestones (Villigen Fm.) by a couple of meters (outcrop 32). **d** A several meter thick damage zone associated with a normal fault cutting through Upper Malm limestone (Villigen Fm.; outcrop 15). See Fig. 1 and in Table 1 for outcrop locations

of the analyzed outcrop types (e.g. road cuts and quarries where joints might have formed due to blasting). Mode-II/in-plane shear fracture types are also joint-like structures but reveal evidence of minor slip increments, e.g. striations or other shear sense indicators (Figs. 2c, d, 4b). Moreover, these fractures also often show vein-like mineralization (Fig. 4b), indicating fluid circulation at depth and excluding recent formation due to relaxation of confining stresses close to the surface or anthropogenic activities. Due to these characteristics, mode-II fractures can certainly be considered to be of structural geological significance and were treated as minor faults in the further course of the fault-slip analysis.

Faults, that according to the definition of Ramsay and Huber (1987) should reveal a measurable amount of displacement (e.g. at least several millimeters), were comparatively rarely observed in the analyzed outcrops, typically at locations in the proximity of major regional or map-scale fault zones. Observed fault offsets were mostly in the centimeter range and only reached more than a meter in a few exceptional cases (Fig. 5). The latter type of brittle

structure was occasionally found to be associated with fault rocks such as cataclastic breccias (Fig. 5c, d).

Figure 6 shows an overview of the present day orientation of all the fractures measured. The compiled dataset, comprising close to 2000 fractures (both mode-II fractures as described above as well as faults), is divided into three areas corresponding to tectonic units, namely the Folded Jura, the Deformed Tabular Jura and the Tabular Jura. For each tectonic unit, rose diagrams are shown for the entire fracture dataset, as well as subsets of sub-vertical (dip angle  $>75^\circ$ ) and dipping fractures (dip angle  $<75^\circ$ ). In all three tectonic units mentioned, N-S to NNE-SSW striking fractures are dominant, particularly when looking only at the sub-vertical fractures (mostly mode-II fractures). They form fairly homogeneous networks consisting of roughly two to three distinct sets. These sets are characterized by differing azimuth orientation, with the constituting fractures being either oriented orthogonally to each other or forming conjugated sets with an intermediate angle of about  $60^\circ$ . The more inclined fractures show a wider range of orientations, whereby NW-SE striking fractures are

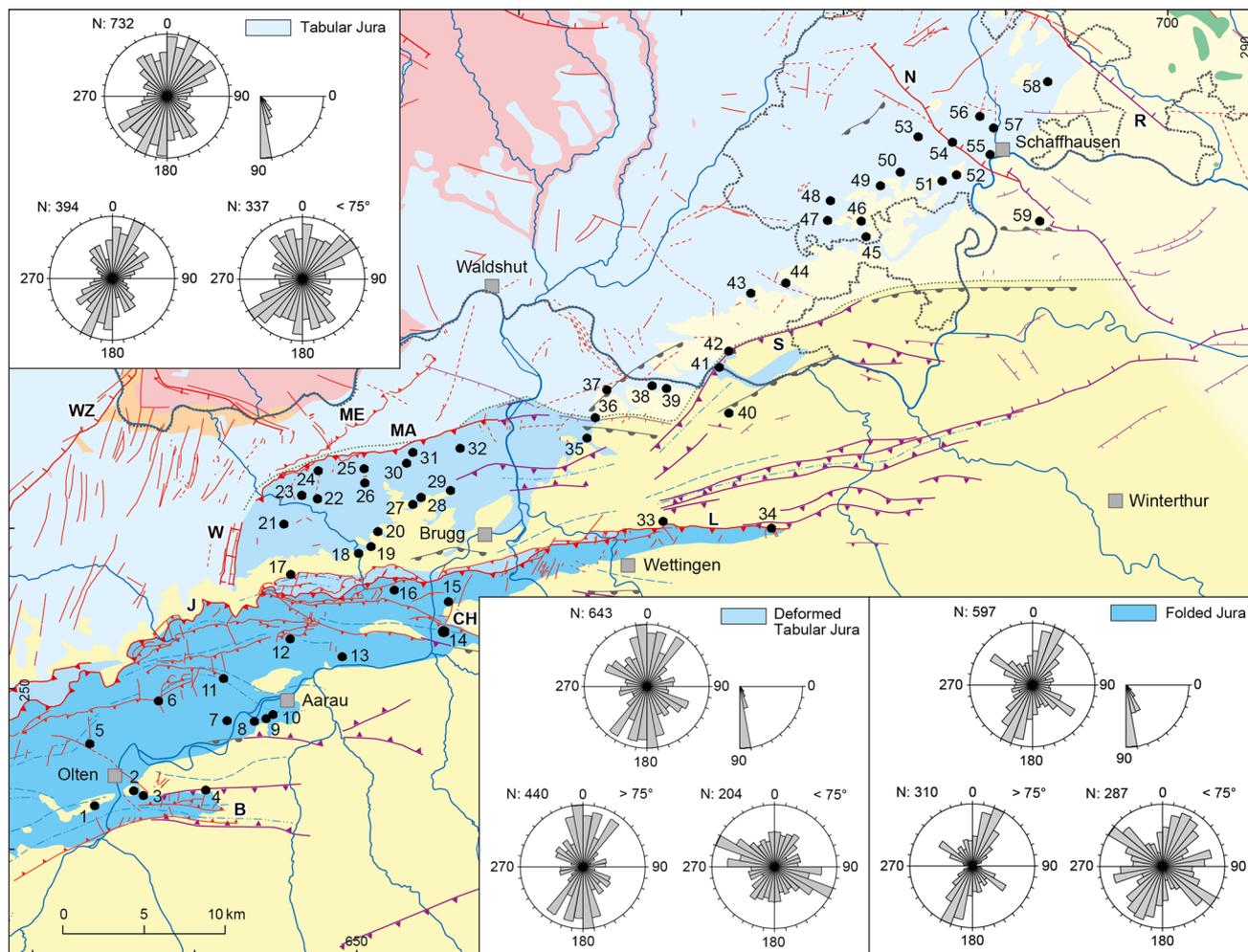


**Fig. 6** Observed fracture orientations separated according to tectonic units. For each unit, rose diagrams for all fractures are shown together with separate plots for steeply (dip angle  $>75^\circ$ ) and moderately to shallowly dipping fractures (dip angle  $<75^\circ$ ).  $N$  number of measurements

particularly common in the Folded Jura and the Deformed Tabular Jura. In the Tabular Jura, but also the Folded Jura, a NE–SW direction is also quite prominently represented. Overall, the obtained fracture orientations are in good agreement with those reported from previous field investigations (Meier 1984; Ramsay and Huber 1987).

Slickolite structures (Fig. 2c) were the shear sense indicators most commonly observed on fracture surfaces whereas calcite growth fibres (Fig. 2d) were only rarely found. Figure 7a shows the relationship between the dip angle of fracture planes and associated shear sense indicators and clearly illustrates the dominance of sub-vertical strike-slip shear fractures. Regarding fracture kinematics, a regional variation in relation to the different tectonic units can be observed (Fig. 7b). The Folded Jura and Deformed Tabular Jura are characterized by the occasional occurrence of reverse faults with dip angles between 20 and 60°. These fractures appear to be particularly common in the vicinity of significant compression structures, such as the

Mandach Thrust, the Jura Main Thrust and the Born-Engelberg Anticline (MA, J and B in Fig. 1 respectively). Towards the east of the study area, normal faults with dips between 50 and 70° occur more frequently and become a common feature in the eastern Tabular Jura, especially near the border faults of the Hegau-Lake Constance Graben (Neuhausen and Randen Faults; N and R in Fig. 1 respectively).

## 4.2 Deformation chronology

### 4.2.1 Formation of bedding-orthogonal joints

The earliest deformation structures observed in the analyzed outcrops are bedding-orthogonal joints without displacement. They are rotated with the sedimentary stack wherever the latter is affected by folding within the Folded Jura and Deformed Tabular Jura (Fig. 8) or tilting in the Tabular Jura. Therefore, the formation of the bedding-

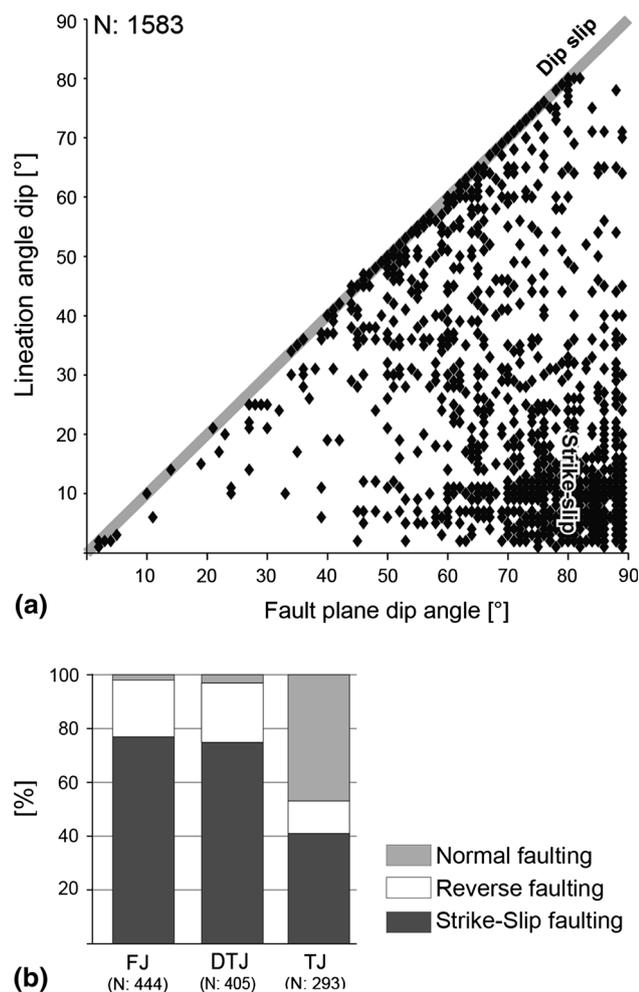


**Fig. 7** Fracture kinematics across the study area: **a** relationship between slip lineation and fracture dip angle for all faults and mode-II fractures discussed. The vast majority of fractures show strike-slip kinematics but dip-slip (reverse and normal faulting) is also common. **b** Distribution of strike-slip, reverse and normal slip indicators according to tectonic units. *FJ* Folded Jura, *DTJ* Deformed Tabular, *TJ* Tabular Jura (compare Figs. 1, 6). *N* number of measurements

orthogonal joints appears to have taken place relatively early and predates the tectonic events responsible for the latter deformations (see discussion in Sect. 5).

#### 4.2.2 Normal faulting in the Eastern Tabular Jura and the Northern Molasse Basin

Normal faulting is observed throughout the study area, but is ubiquitous in every outcrop in the easternmost part of the investigation area. Here, two different sets of normal faults are observed striking NE–SW and NW–SE to NNW–SSE (see rose diagrams in Fig. 6). No clear relative age relationship could be established between these two different sets of normal faults, suggesting that they may have developed contemporaneously (see further discussion in

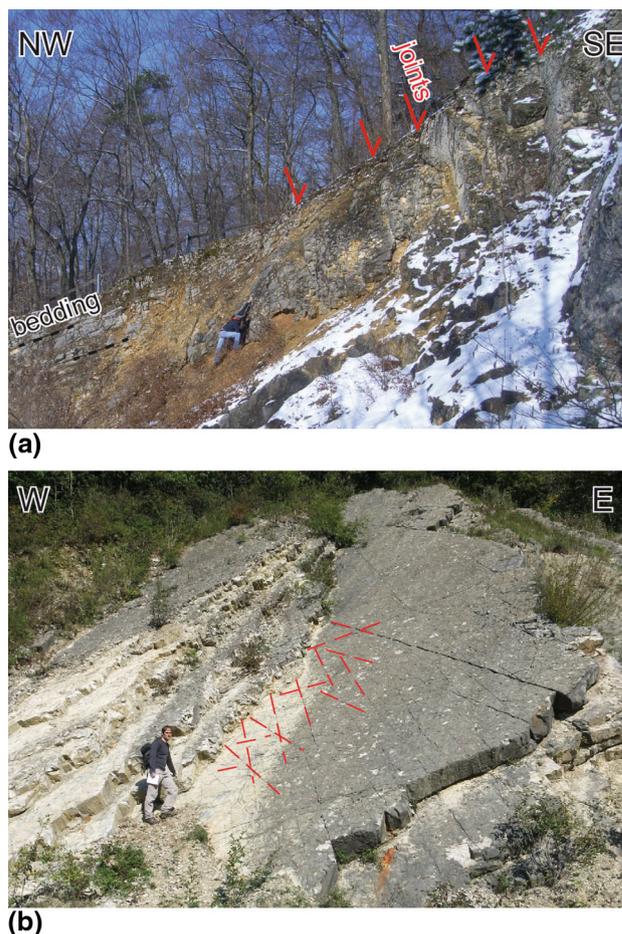
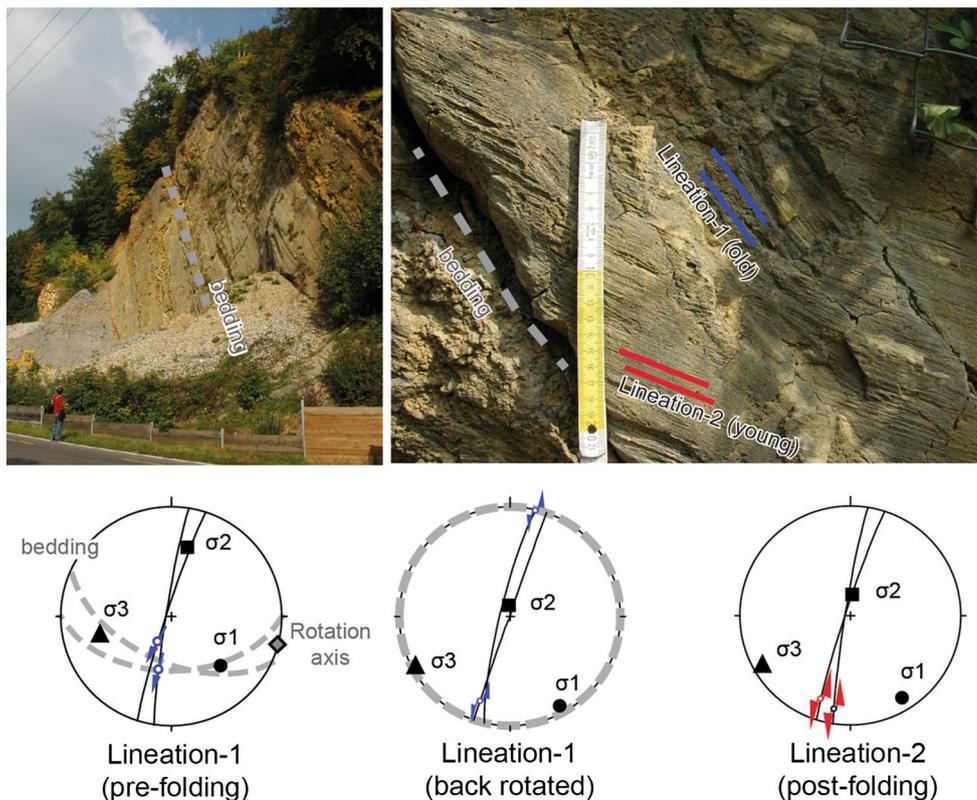


**Fig. 8** Rotation of bedding-orthogonal fractures in outcrops within the Folded Jura. **a** NNE–SSW directed view of an outcrop face exposing northwards dipping Upper Malm limestone (Villigen Fm.; outcrop 3) at the northern limb of the Born-Engelberg Anticline (B in Fig. 1). **b** N–S directed view onto folded Malm limestones (Wildeggen Fm.; outcrop 14) forming the back-limb of the Chestenberg Thrust (CH in Fig. 1). See Fig. 1 and in Table 1 for outcrop locations

Sect. 4.3.1). Isolated signs of normal faulting were also recorded across the rest of the study area, in particular southeast of Waldshut (Fig. 1).

The timing of onset of normal faulting is not well constrained. However, the normal faults were often found to offset bedding-orthogonal joints. Therefore, they are considered to be relatively younger. Additional relative chronology criteria such as cross-cutting fracture planes (e.g. Fig. 3) and occasionally observed overprinting shear sense indicators allow the temporal relationships between normal faulting and other brittle structures to be evaluated. Accordingly, normal faulting predates strike-slip faulting along reactivated bedding orthogonal joints described below. In the northeastern part of the study area similar normal faults were also recognized in exposures of sediments belonging to the Upper Marine Molasse (Burdigalian according to Hofmann and Hantke 1964; compare Fig. 5b).

**Fig. 9** Indications for rotation of a strike-slip fault cutting through folded Middle Jurassic limestones in the Folded Jura (Hauptrogenstein Fm.; outcrop 12, see in Fig. 1; Table 1 for location). After rotation of the fault-slip dataset by the bedding dip angle, calculated stress axes are in line with the Andersonian model (see text for discussion). Note that the fault plane also shows signs of post-folding strike-slip movement (*Lineation 2*), indicating no major changes in fault-slip kinematics and orientation of stress axes between folding. Fracture data are illustrated as lower hemisphere equal area projections



At least in this area, extensional deformation therefore postdates Early Miocene times.

#### 4.2.3 Regional strike-slip faulting along bedding orthogonal joints before and during Jura folding

Minor sub-vertical strike-slip faults are the most widely recognized brittle deformation structures throughout the study area. The locally observed fracture geometries suggest that most of these strike-slip faults represent reactivated joints. However, the formation of new sub-vertical fractures during this deformation phase cannot be excluded.

In the northeastern part of the study area (e.g. the Tabular Jura), cross-cutting and overprinting criteria between strike-slip faults and normal faults indicate that strike-slip faulting initiated after normal faulting (Fig. 3). Along the Jura fold-and-thrust belt, where the sedimentary stack is commonly folded, bedding-orthogonal strike-slip striations reactivating former joints are very frequently found to be rotated together with the folded strata (Fig. 9). Moreover, strike-slip faults are often offset along bedding planes affected by flexural slip in these areas. These observations imply that this strike-slip faulting initiated prior to folding and hence the main deformation associated with the formation of the Jura fold-and-thrust belt. Becker's (2000) suggestion that the formation of the thin-

skinned Jura Mountains commenced in the Early Miocene, at the earliest around 12 Ma, yields a first constraint regarding the minimum age for the onset of strike-slip faulting (see further discussion in Sect. 5.5). In Fig. 9, the second, sub-horizontal set of striations indicates that strike-slip movements along this set of sub-vertical fractures continued throughout the course of the folding and hence were continuously active during Jura folding.

#### 4.2.4 Reverse faulting, folding and flexural slip across the Folded and Deformed Tabular Jura

Reverse faulting, folding and flexural slip within the Jura Fold-and-Thrust Belt often appear to post-date the strike-slip faulting described above. At many locations, the reverse faults terminate at the intersection with sub-vertical strike-slip faults. Such geometric relationships suggest that the reverse faults postdate at least some of the strike-slip faults (Meier and Kronberg 1989). This interpretation is in line with the observation that strike-slip faults were often rotated during folding in which case they pre-date the main phase of Jura folding.

#### 4.2.5 Strike-slip faulting post-dating folding

Strike-slip faulting along sub-vertical fractures post-dating the main folding phase along the Jura Fold-and-Thrust Belt

was also occasionally recognized. Most often, signs of such young increments of strike-slip movement were found to result from reactivation of pre-existing fractures (Fig. 9). Newly formed strike-slip faults that can be identified when cutting straight through folded strata were observed only rarely (Fig. 10) but suggest that strike-slip deformation outlasted the main phase of Jura folding.

### 4.3 Regional fault-slip analysis

Fault-slip analyses were carried out separately for each individual outcrop. At this scale, the separation of the fracture data into kinematically homogeneous subsets relies directly on field observations for the most part, rather than on the often ambiguous results of graphical separation tests. In the following, the results of fault slip analyses from the individual outcrops are integrated and discussed at the regional scale.

#### 4.3.1 Post Early Miocene extension

In the northeastern part of the study area close to the border faults of the Hegau-Lake Constance Graben (e.g. the

**Fig. 11** Results of fault-slip analyses across northern Switzerland showing local indications of extension. Symbols indicate the orientation of the minimum horizontal stress axis ( $\sigma_3$ ). Numbers refer to the outcrops listed in Tables 1 and 2. The fracture datasets underlying the fault-slip analyses are shown as lower hemisphere equal area projections. Note that the datasets at the locations southeast of Waldshut are poor and merely shown for discussion purposes

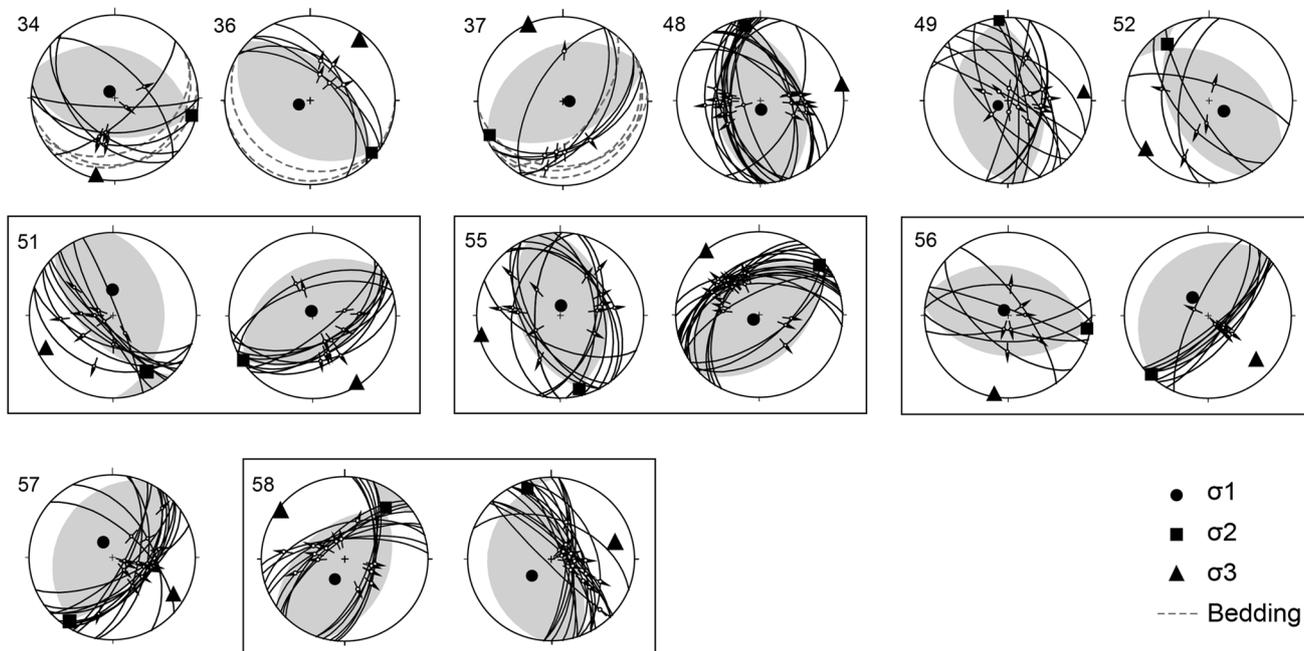
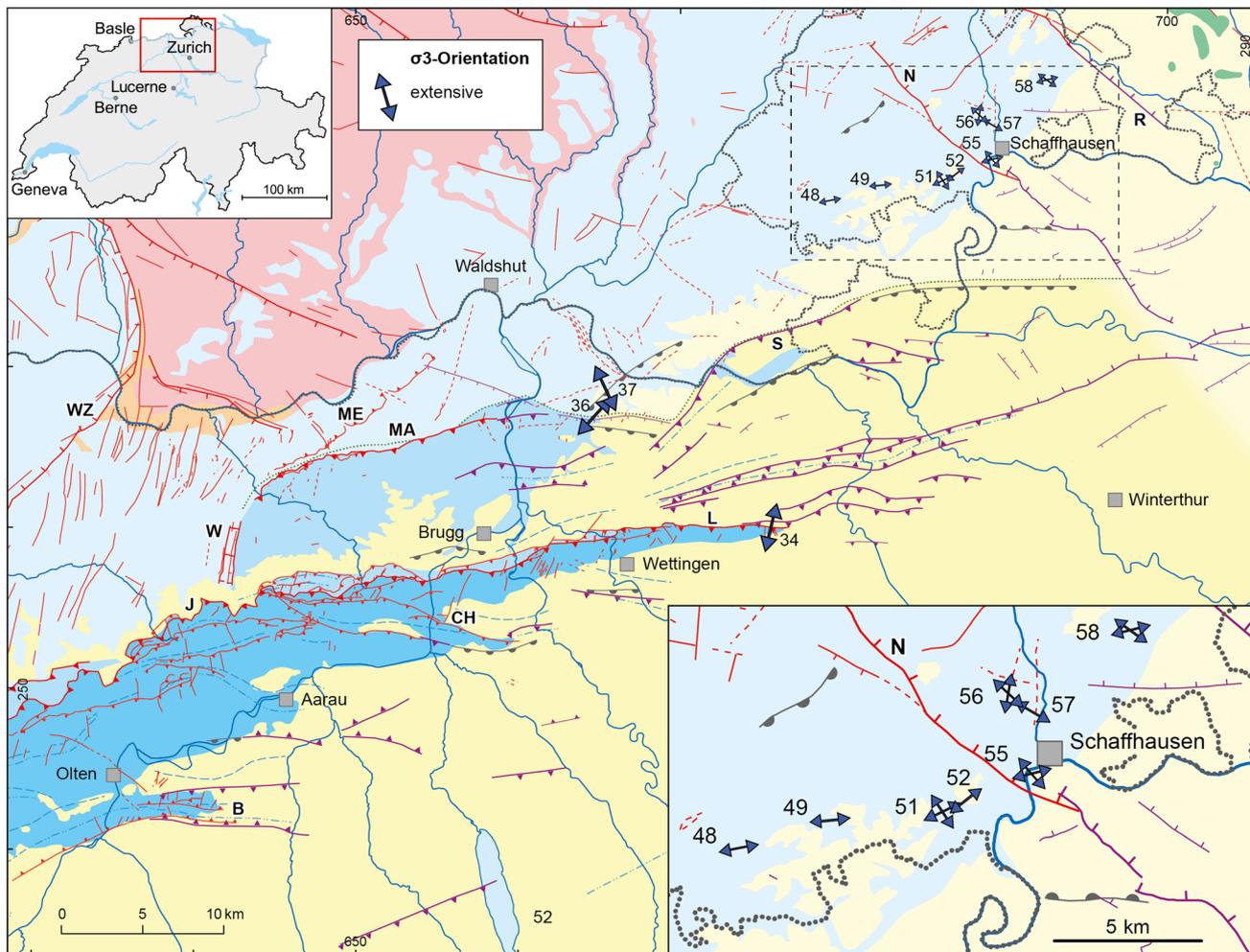
Neuhausen and Randen Faults, N and R in Fig. 11) the fault slip analyses yield reliable indications for extension at several locations (Fig. 11). Two different orientations of the minimum principal stress axis ( $\sigma_3$ ) are observed striking ENE–WSW and NW–SE respectively. Combining the two stress tensors, considering that the associated fault sets apparently formed contemporaneously (see Sect. 4.2.2), would result in a tectonic regime close to radial extension at some locations (Fig. 11). Extensional deformation in this area can be reliably inferred to postdate Early Miocene times (see Sect. 4.2.2) but predates regionally observed strike-slip deformation (see Sect. 4.2.3).

Much less robust indications of extension are also found further to the west, southeast of Waldshut (e.g. outcrops 36 and 37; Fig. 11). In this area the orientation of  $\sigma_3$  is roughly perpendicular to the trend of neighboring map-scale flexures (see Fig. 11). It is unclear if these indications



**Fig. 10** Indications for post-folding strike-slip faulting at the front of the Folded Jura. A NNW–SSE striking fracture showing horizontal striations cuts straight through overturned limestone beds of Middle

Jurassic limestone (Hauptrogenstein Fm.; outcrop 17, see Fig. 1; Table 1 for location)



of extension and associated normal faults relate to the same post Early Miocene tectonic event as the normal faults found frequently further to the east (see discussion in Sect. 5). Further to the southwest normal faults were not recorded frequently enough to allow for a robust fault-slip analysis and reconstruction of a reliable paleostress tensor.

#### 4.3.2 Late Miocene shortening

This shortening event is recorded over the entire study area (Figs. 12, 13). At the vast majority of locations the reconstructed maximum principal stress axes ( $\sigma_1$ ) trend NW–SE to NNE–SSW. Most often the orientation of  $\sigma_1$  is manifested by sub-vertical, conjugated strike-slip faults trending N–S to NNE–SSW (sinistral) and NW–SE to WNW–ESE (dextral; e.g. locations 8, 27, 43 in Figs. 12, 13). Within the Jura Fold-and-Thrust Belt (e.g. the Folded

Jura and the Deformed Tabular Jura), reverse faults are also observed. With few exceptions (compare Fig. 14) these reverse faults are kinematically compatible with the strike-slip faults and define local tectonic regimes of transpression (e.g. locations 6, 18, 35 in Figs. 12, 13) and where dominant compression (e.g. locations 17 in Figs. 12, 13).

NW–SSE to NW–SE shortening initiated after the formation of outcrop-scale normal faults but before the formation of the map-scale compressional structures related to the easternmost Jura Fold-and-Thrust Belt, which is constrained by the consistent rotation of the shortening defining strike-slip faults in folded areas. Shortening directions obtained from the occasionally recorded post-folding strike-slip fault increments show no deviation in the orientation of  $\sigma_1$  (see Figs. 9, 13). With very few exceptions (compare Fig. 14) no distinction between a pre- and post-folding stress state is possible.

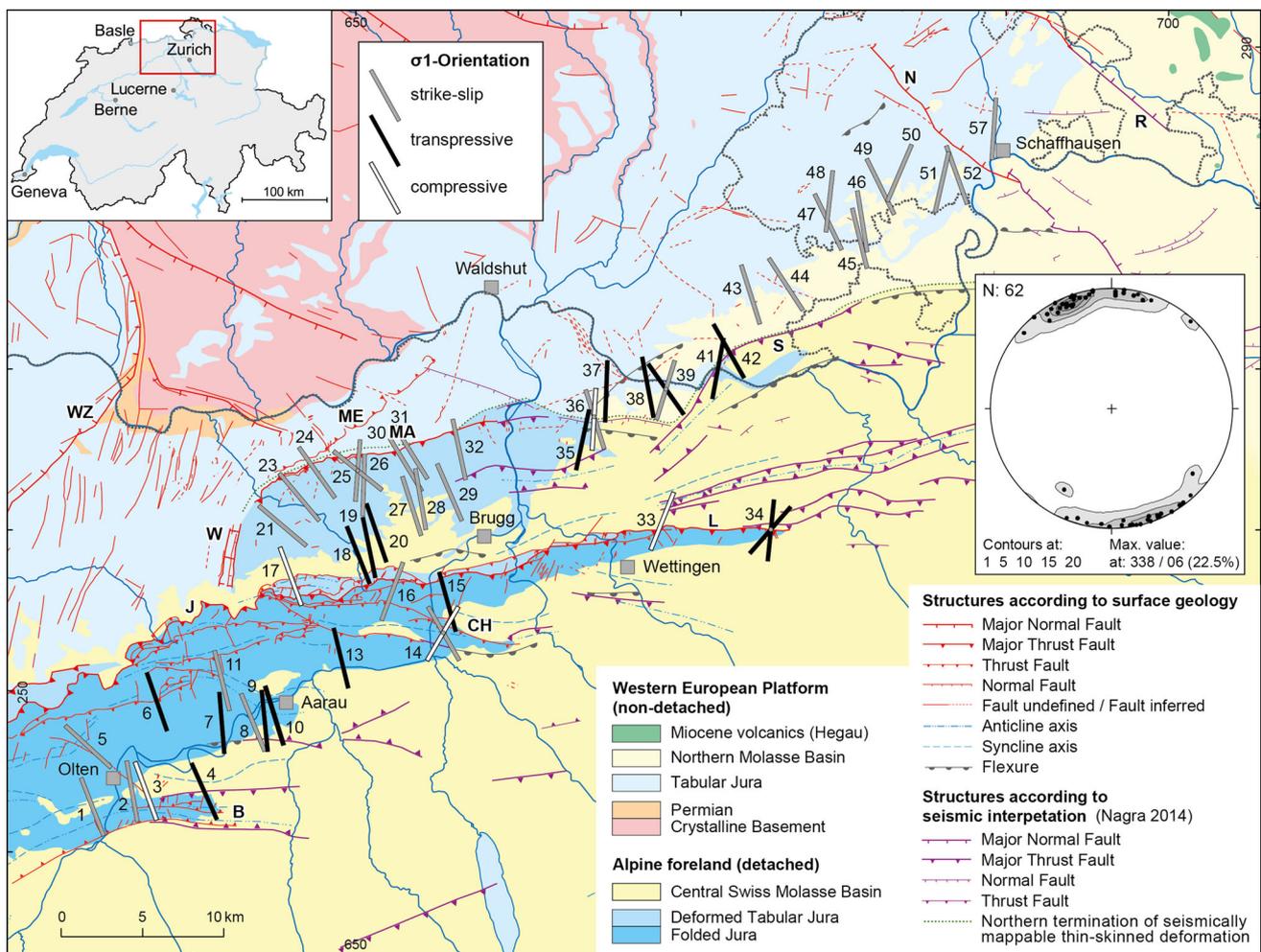


**Fig. 12** Results of fault-slip analyses across northern Switzerland showing regionally well constrained Late Miocene shortening. *Bars* show the orientation of the maximum horizontal stress axis ( $\sigma_1$ ), scales of *grey* indicating the tectonic regime. The contoured plot of all reconstructed  $\sigma_1$  axes shows that on the regional scale,  $\sigma_1$  trends

roughly NW–SE to NNW–SSE but NNE–SSW to NE–SW orientations are also observed (see text for discussion). *Numbers* refer to the outcrops listed in Tables 1 and 3. The fracture datasets underlying the fault-slip analyses are shown in Fig. 13 for selected outcrops

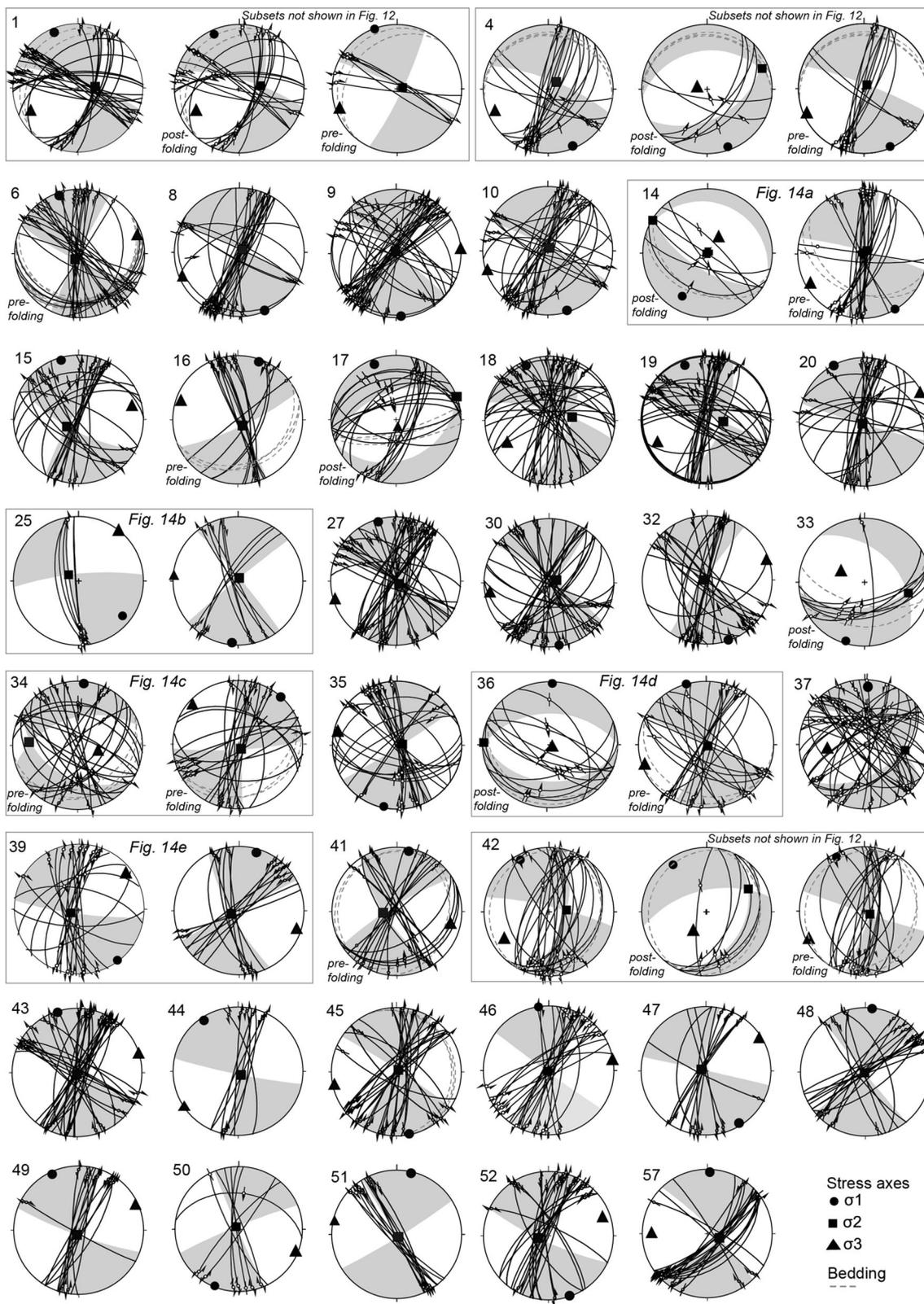


**Fig. 13** Lower hemisphere equal area projections of fault-slip pairs and according results of Right-Dihedra fault-slip analyses for selected outcrops with indications of Late Miocene shortening (compare

Tables 1, 3; Fig. 12). Note the fracture subsets shown in boxes for selected outcrops, some of which are further discussed in Fig. 14

**Table 2** Outcrops where fault-slip analysis yielded indications of extension (compare Fig. 11)

Outcrop signature	N	n	Right-Dihedra fault-slip analysis						Tectonic regime	Age constraint
			$\sigma_1$		$\sigma_2$		$\sigma_3$			
			Azi.	Pl.	Azi.	Pl.	Azi.	Pl.		
34	7	0	322	82	103	6	194	5	Extension	Pre-tilting
36	5	1	219	72	311	1	42	18	Extension	Pre-tilting
37	6	3	352	80	246	3	156	10	Extension	Post-tilting
48	20	4	175	81	349	9	79	1	Extension	Post-tilting
49	14	2	245	79	353	3	84	10	Extension	
51	10	2	359	65	149	22	244	11	Extension	
51	11	3	348	85	237	2	147	4	Extension	
52	5	0	126	72	324	17	232	5	Extension	Post-tilting
55	14	0	5	80	166	9	256	3	Extension	
55	19	0	228	23	50	7	320	0	Extension	
56	7	0	321	84	100	5	190	4	Extension	
56	9	0	320	67	224	3	133	23	Extension	
57	16	2	330	73	213	8	121	5	Extension	
58	15	0	205	68	38	22	306	5	Extension	
58	18	2	228	65	342	11	76	22	Extension	

$N$  number of relevant fracture measurements,  $n$  number of fracture measurements with no shear sense information.  $\sigma_1 > \sigma_2 > \sigma_3$  maximum, intermediate and minimum principal stress axes,  $Azi$  Azimuth,  $Pl.$  Plunge

**Table 3** Outcrops where fault-slip analysis yielded indications of shortening (compare Figs. 12, 13)

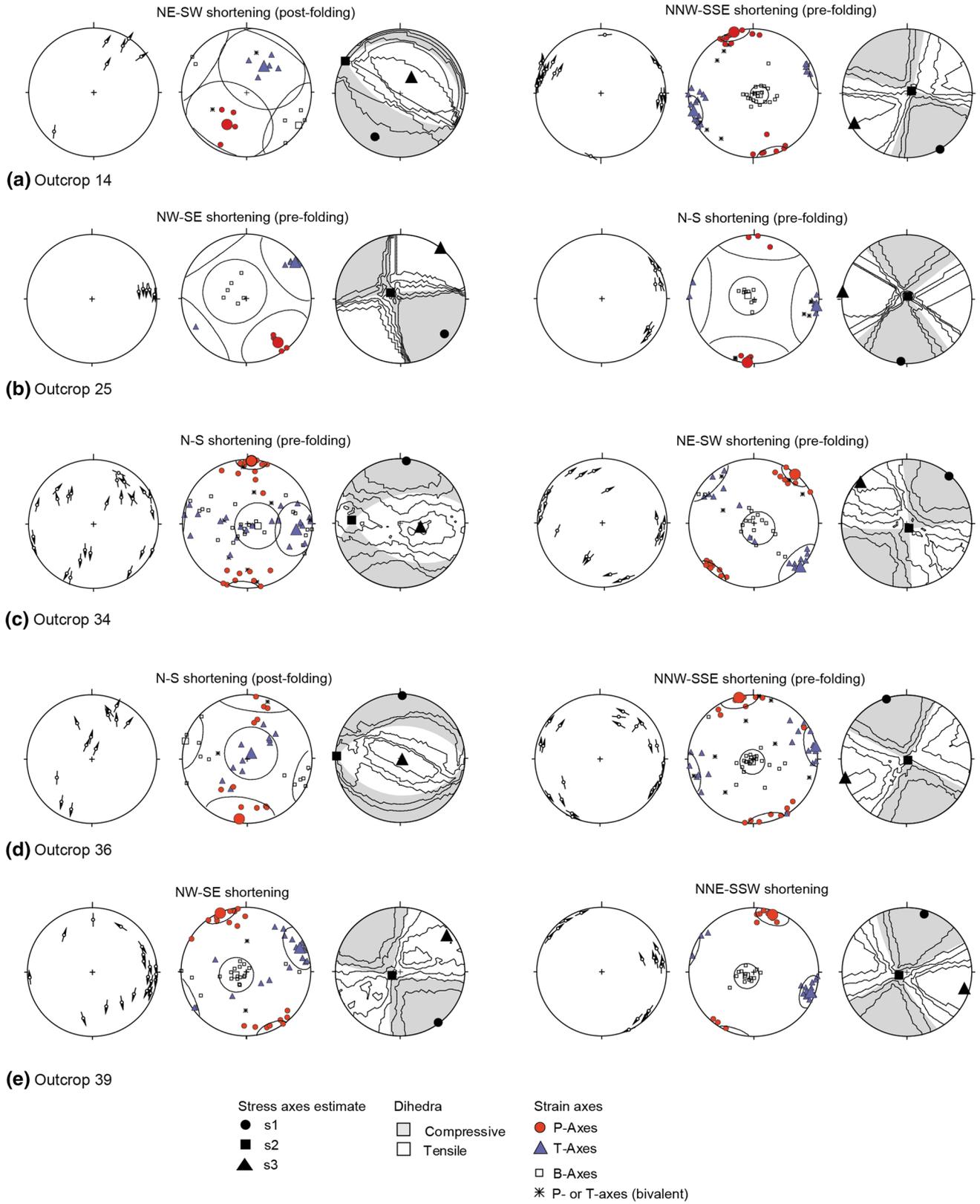
Outcrop signature	N	n	Right-Dihedra fault-slip analysis						Tectonic regime	Age constraint
			$\sigma_1$		$\sigma_2$		$\sigma_3$			
			Azi.	Pl.	Azi.	Pl.	Azi.	Pl.		
1	27	1	337	7	86	68	244	21	Strike-slip	Pre- to post folding
1	21	1	336	9	82	62	242	27	Transpression	Post-folding
1	6	0	340	2	81	82	250	8	Strike-slip	Pre-folding
2	33	3	170	2	53	86	260	3	Strike-slip	Pre-folding
3	16	4	340	9	71	7	198	79	Compression	Pre- to post folding
4	18	0	157	4	49	77	248	13	Transpression	Pre- to post folding
4	6	0	161	6	69	11	278	77	Compression	Post-folding
4	12	0	156	3	37	84	246	5	Strike-slip	Pre-folding
5	21	5	341	0	246	86	71	4	Strike-slip	Pre- to post folding
6	32	3	341	5	217	81	72	8	Transpression	Pre-folding
7	21	2	174	7	35	81	256	6	Transpression	
8	29	4	157	2	48	85	247	5	Strike-slip	
9	41	1	175	3	346	87	85	0	Transpression	
10	32	0	162	3	29	86	252	3	Transpression	
11	10	2	166	0	72	82	256	8	Strike-slip	Pre-folding
13	9	2	347	6	83	48	252	42	Transpression	Pre-folding
14	6	1	210	23	301	3	37	67	Compression	Post-folding
14	22	4	150	0	57	84	240	6	Strike-slip	Pre-folding
15	23	4	344	5	238	73	75	16	Transpression	
16	14	2	20	5	139	81	289	8	Strike-slip	Pre-folding
17	19	6	339	9	69	1	166	81	Compression	Post-folding
18	34	3	337	8	81	62	243	27	Transpression	
19	37	0	339	10	96	68	246	19	Transpression	

**Table 3** continued

Outcrop signature	N	n	Right-Dihedra fault-slip analysis						Tectonic regime	Age constraint
			$\sigma 1$		$\sigma 2$		$\sigma 3$			
			Azi.	Pl.	Azi.	Pl.	Azi.	Pl.		
20	23	6	332	1	282	87	62	3	Transpression	
21	11	0	311	5	193	80	41	9	Strike-slip	
22	17	1	138	3	348	87	229	1	Strike-slip	
23	21	1	320	1	101	89	230	1	Strike-slip	
24	15	3	145	2	259	85	55	4	Strike-slip	Pre- to post-folding
25	6	0	129	15	302	75	38	2	Strike-slip	Pre-folding
25	9	3	185	4	21	86	275	1	Strike-slip	Pre-folding
26	10	1	181	2	360	88	91	0	Strike-slip	
27	39	5	344	5	129	84	254	3	Strike-slip	
28	14	3	351	2	133	88	261	1	Strike-slip	Post-folding
29	17	2	337	6	212	79	68	9	Strike-slip	
30	30	0	171	2	68	81	261	9	Strike-slip	
31	9	1	329	4	188	85	59	3	Strike-slip	Pre-folding
32	41	1	170	2	284	86	80	3	Strike-slip	
33	8	3	197	5	104	32	295	58	Compression	Post-folding
34	26	4	6	4	274	26	104	64	Transpression	Pre-folding
34	20	3	42	3	154	30	311	6	Transpression	Pre-folding
35	30	2	192	3	78	83	282	7	Transpression	
36	12	1	2	3	272	2	143	86	Compression	Post-folding
36	22	4	342	2	119	88	252	2	Strike-slip	Pre-folding
37	41	5	2	7	98	40	263	49	Transpression	Post-folding
38	26	2	349	4	249	66	81	23	Transpression	Post-folding
39	20	1	143	2	245	79	53	11	Transpression	
39	14	0	16	7	248	79	107	8	Strike-slip	
41	22	10	11	5	264	73	103	16	Transpression	Pre-folding
42	25	6	331	10	86	68	238	20	Transpression	Pre- to post folding
42	<i>6</i>	<i>1</i>	<i>325</i>	<i>12</i>	<i>62</i>	<i>26</i>	<i>213</i>	<i>60</i>	<i>Compression</i>	<i>Post-folding</i>
42	<i>19</i>	<i>5</i>	<i>333</i>	<i>7</i>	<i>120</i>	<i>82</i>	<i>243</i>	<i>4</i>	<i>Strike-slip</i>	<i>Pre-folding</i>
43	34	0	342	2	181	88	72	1	Strike-slip	
44	8	0	326	6	143	84	236	0	Strike-slip	
45	28	3	168	0	261	83	78	7	Strike-slip	
46	23	1	351	1	237	88	81	2	Strike-slip	
47	12	2	155	4	278	83	64	6	Strike-slip	
48	19	4	6	1	226	89	96	1	Strike-slip	Post-tilting
49	13	0	335	5	199	84	65	4	Strike-slip	
50	9	2	202	2	318	86	112	4	Strike-slip	
51	13	1	13	3	157	86	283	3	Strike-slip	
52	23	1	161	1	257	77	70	13	Strike-slip	Post-tilting
57	20	4	2	5	110	74	271	15	Strike-slip	Post-tilting

Italic letters show fault-slip analyses for fracture subsets representing pre- and post folding states of deformations that yielded identical results (compare Fig. 13)

*N* number of relevant fracture measurements, *n* number of fracture measurements with no shear sense information.  $\sigma 1 > \sigma 2 > \sigma 3$  maximum, intermediate and minimum principal stress axes, *Azi* Azimuth, *Pl.* Plunge



◀**Fig. 14** Illustration of fault-slip analysis for five selected outcrops where NW–SE to NNW–SSE as well as NNE–SSW to NE–SW Late Miocene shortening directions were reconstructed (compare Fig. 12). Sub-figures **a** to **e** show the two fault-slip subsets for the different outcrops respectively (*numbers on the left side* refer to Tables 1, 3 and Fig. 1). For each subset the fault-lineation pair is shown as tangent-lineation and P–T axis plot together with contoured dihedral angles and principal stress axes estimates stemming from the fault-slip analysis (compare Fig. 13). **a** Distinctively differing shortening directions derived from pre- and post-folding fault-slip data close to a major thrust fault in the Folded Jura. **b** Differing orientation of shortening directions most likely due to poor kinematic fracture data underlying the fault-slip analysis. **c** Differing shortening directions close to a major thrust fault in the Folded Jura. **d, e** Marginally differing shortening directions between fault-slip data at the front of the Deformed Tabular Jura

On the regional scale, the NW–SE to NNE–SSW orientation of  $\sigma_1$  is quite consistent to the south of the Folded Jura and again in the Eastern Tabular Jura. In between these areas, a slight change in orientation of  $\sigma_1$  can be inferred along the front of the Folded Jura and the Deformed Tabular Jura. In the westernmost part of the Deformed Tabular Jura,  $\sigma_1$  trends NW–SE, while in the eastern part its orientation trend is rather N–S. This observation indicates a subtle clockwise rotation of  $\sigma_1$  from west to east (Fig. 12), which is in good agreement with the results of previous investigations (Hindle and Burkhard 1999; Homberg et al. 2002).

As illustrated in Figs. 12 and 13,  $\sigma_1$  is occasionally oriented NNE–SSW to even NE–SW. Only in a very few cases could NNE–SSW to NE–SW shortening be reconstructed in addition to widely recognized NW–SE to NNW–SSE shortening at the same location (locations 14, 25, 34, 39 in Figs. 12, 13 and 14a–c, e). The data separation underlying these reconstructions was mostly based on graphical tests for kinematic homogeneity with no clear field evidence yielding indications for relative chronology (e.g. as shown in Fig. 3). It is interesting to note that, in most cases where N–S to NE–SW shortening was recorded within the Jura Fold-and-Thrust Belt (e.g. the Folded and Deformed Tabular Jura),  $\sigma_1$  is oriented roughly perpendicular to the trend of major adjacent compression structures such as thrust faults and anticline axes (e.g. location 14, 35 in Fig. 12). Elsewhere, the fault-slip datasets underlying the reconstruction of NNE–SSW to NE–SW shortening are often rather poor (e.g. unidirectional data such as at locations 16, 25, 51 in Figs. 13 and 14b), speaking for a cautious tectonic interpretation in terms of a regional tectonic stress field (also compare Sect. 5.2).

## 5 Discussion

In this section the interpretations outlined above are discussed in the context of the wider region's tectonic history (Fig. 15). The imprint of the major Latest Mesozoic and Cenozoic tectonic events on the outcrop-scale fracture systems of the study area is examined.

### 5.1 Latest Mesozoic to Eocene uplift of the Alpine foreland

Uplift of several 100 m related to the establishment of the Alpine forebulge in central northern Switzerland is evidenced by the pronounced erosional unconformity marking the Mesozoic–Cenozoic boundary (Müller et al. 2002) and by fission track data (Mazurek et al. 2006; Timar-Geng et al. 2006). Crustal uplift involving the reduction of confining stress in the rock column parallel to the bedding favors the formation of bedding-orthogonal joints (Mandl 2005 with references therein) such as those widely observed across the entire study area. Hence, the majority of these fractures may well have already formed during this latest Mesozoic to Eocene uplift stage. This interpretation is in line with the observation that the bedding-orthogonal fractures appear to pre-date all other observed brittle deformation features (compare Sect. 4.2).

### 5.2 Eocene–Oligocene formation of the Upper Rhine Graben

E–W to WNW–ESE extension leading to the opening of the Upper Rhine Graben began during Late Eocene to Early Oligocene times (Hinsken et al. 2007). If the opening of the graben had a significant tectonic effect on the study area, this should be evidenced by the fracture characteristics in the analyzed outcrops of Jurassic limestones (e.g. occurrence of normal faults indicating E–W extension). Theoretically, the widely recognized N–S striking sub-vertical joints could be related to an extensional event. Also, the map-scale flexures north of the Folded Jura could be caused by extensional faulting related to the formation of the Upper Rhine Graben. The kinematic analyses of outcrop-scale fractures, however, showed no significant imprint of presumably E–W directed Eo-Oligocene extension. Despite some very favorable outcrops in the western half of the study area, indications for E–W extension are very rare and no robust associated paleostress state can be reconstructed. Hence, the imprint of Upper Rhine Graben-related extension on the area of interest was very minor. It appears that stronger effects of E–W oriented extension related to the opening of the Graben are only observable to the west of the study area, beyond the Wölflinswil Graben and the Wehra-Zeiningen-Fault (W and WZ in Fig. 1, respectively).

### 5.3 Late Oligocene/Early Miocene uplift of the Black Forest Massif and subsidence of the Molasse basin

The interpretation of reflection seismic data across the study area suggests that Late Oligocene/Early Miocene

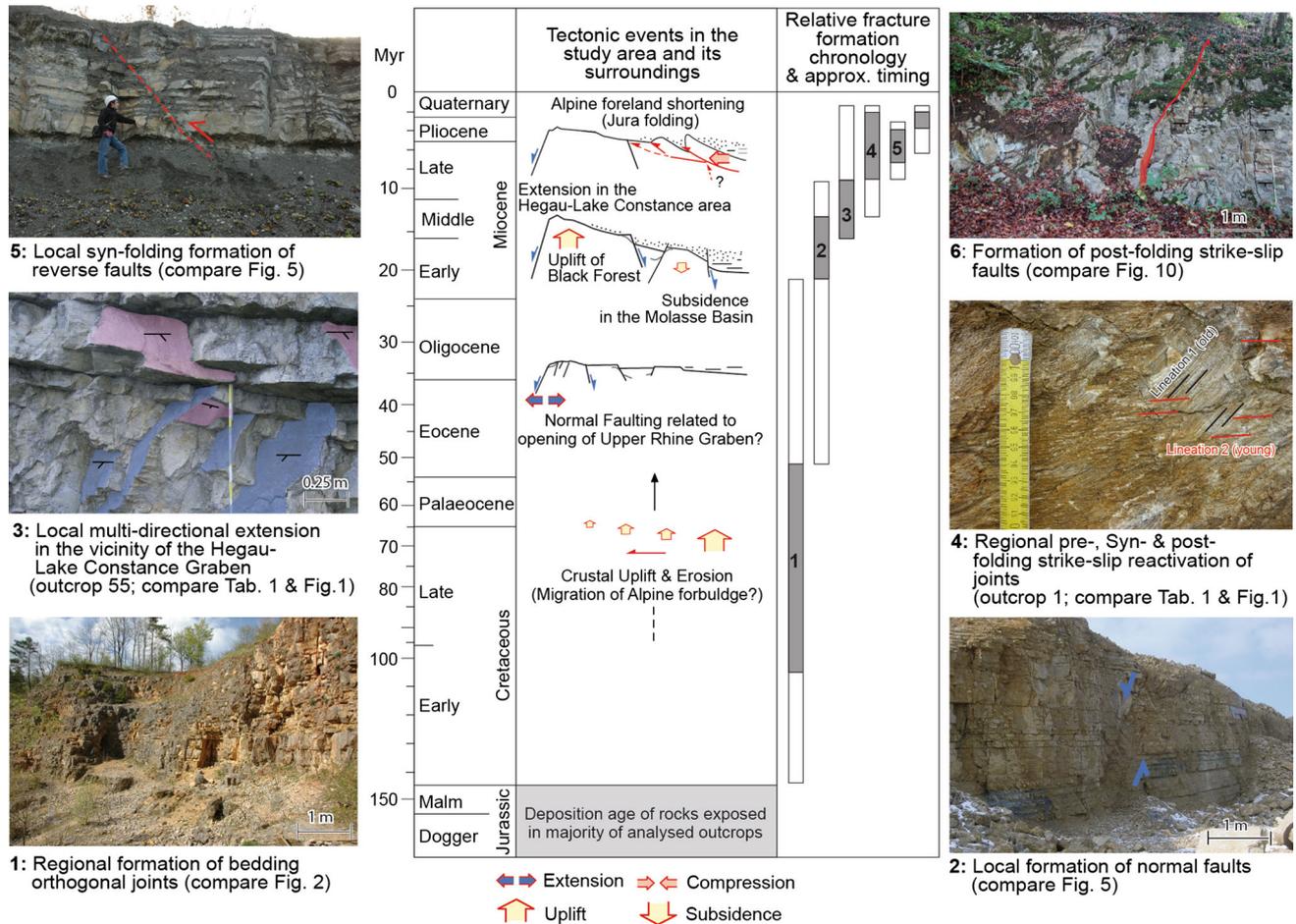


**Fig. 15** Synopsis of study results showing the relative chronology of observed fracture systems in relation to regionally recognized tectonic events within and around the study area (see text for discussion). The numbering of fracture sets indicates their relative chronology from 1

(oldest) to 6 (youngest). White bars indicate the possible formation timeframe for the different fracture sets, grey bars show the preferred interpretation

uplift of the Black Forest Massif and contemporaneous subsidence of the southward adjacent Swiss Molasse Basin were associated with formation of flexures of the sedimentary stack above reactivated basement faults (Naef et al. 1995; Diebold and Noack 1997; see the indicated flexures in Fig. 1). The analyzed outcrops in the vicinity of such flexures quite typically show signs of normal faulting, although not frequently enough to support the robust deduction of a paleostress tensor (Fig. 11). As a consequence, it is concluded that the uplift of the Black Forest and subsidence of the Molasse Basin had only local effects on the outcrop-scale fracture pattern. The imprint appears to be strongest in the immediate vicinity of major fault zones, for example southeast of Waldshut (Fig. 11).

As indicated in Fig. 15, the bedding-orthogonal joint systems observable throughout the area could also be related to this deformation event. However, the author's

preferred interpretation is that the formation of these fractures already took place during the Latest Mesozoic to Eocene uplift phase (compare Sect. 5.1).

#### 5.4 Post Early Miocene formation of the Hegau-Lake Constance Graben

Outcrop-scale normal faults are particularly common in the northeastern part of the investigation area. They apparently formed after the deposition of Early Miocene sediments belonging to the Upper Marine Molasse (see Sect. 4.2.2 and Fig. 5b). It seems plausible to directly relate the observed outcrop deformation features with the evolution of the neighboring crustal-scale fault zone of the Hegau-Lake Constance Graben whose main deformation activity is also inferred to postdate Early Miocene times (Schreiner 1992; Hofmann et al. 2000; Ibele 2015).

The outcrop-scale deformation pattern is particularly complex in the area of Schaffhausen (Fig. 11). NE–SW extension perpendicular to the trend of the major normal faults is accompanied by NW–SE to NNW–SSE extension oriented parallel to the mentioned normal faults and leads locally to a tectonic regime close to radial extension (Fig. 11). The interpretation of NW–SE to NNW–SSE extension at the outcrop scale is not straightforward but appears to be a local phenomenon, most likely representing strain field perturbations in the vicinity of the border faults of the Hegau-Lake Constance Graben (e.g. the Neuhausen and Randen Faults, N and R in Fig. 11). Similar stress states of radial extension were observed along the southern and northern edges of the Upper Rhine and Bresse Grabens respectively, where these roughly N–S trending structures intersect with the ENE–WSW trending Paleozoic troughs of Northern Switzerland and Burgundy (Ustaszewski et al. 2005; Madritsch et al. 2009). In these areas, radial extension was explained by the structural inheritance and reactivation of the pre-existing Paleozoic basement structures oriented perpendicular to the overall extension direction. A similar interpretation could be considered for the study area south of Schaffhausen (Fig. 11) where the roughly E–W striking crystalline Benken Horst forms a major subsurface basement structure (Müller et al. 2002). Reactivation of its ENE–WSW striking border faults during Cenozoic times could also possibly explain the observed NNW–SSE oriented extension directions.

### 5.5 Late Miocene formation of the Jura Fold-and-Thrust Belt

This tectonic event had the strongest imprint on the outcrop-scale fracture systems of the area. It is represented by strike-slip and reverse faults. Notably, at a few locations within the Jura Fold-and-Thrust Belt, Madritsch and Hammer (2012) also recorded normal faults that apparently formed in relation to map-scale fold structures; however these faults were not found frequently enough to allow a fault-slip analysis.

Fault-slip analyses allow this deformation event to be divided into two phases. In the first phase, NW–SE compression resulted in the initiation of strike-slip faulting, frequently along pre-existing joints. This deformation phase is traceable into the Tabular Jura and most likely marks the onset of the Alpine collision-related deformation in this area. It starts prior to the main phase of the formation of the Jura Fold-and-Thrust Belt, as is clearly indicated by the rotation of associated fractures in the areas affected by folding. Rittner (2013) provides a single U–Pb age of  $9 \pm 0.94$  Ma for a pre-folding slickenside from outcrop 1 (compare Fig. 2d). Considering the relative

chronology of deformation established earlier (Sect. 4.2), this age would represent the maximum age for the onset of folding in the easternmost Jura Fold-and-Thrust Belt. This is a rather young maximum age but still in good agreement with stratigraphic and paleontological constraints (Becker 2000) and geomorphic observations (Ziegler and Fraefel 2009). The second deformation phase is considered to reflect the actual formation of the easternmost Jura Fold-and-Thrust Belt during which the pre-existing strike-slip faults were reactivated (Fig. 9), most likely simultaneously with the development of newly formed reverse faults. In the western part of the study area, no stress field changes associated with the formation of folds and thrusts are recognizable (see Fig. 13).

As discussed in Sect. 4.3.2, the tectonic interpretation of the locally recognized NNE–SSW to NE–SW orientation of  $\sigma_1$  needs to be treated with caution. The fact that these shortening directions were only recognized together with the dominant NW–SE to NNW–SSE shortening at the same location in very few cases (Figs. 12, 13 and 14) and the separation of the underlying fault-slip data mostly relied on graphical homogeneity tests rather than direct field observations speaks against the interpretation of two individual Miocene shortening events and two different paleostress fields. In fact, towards the east of the study area, the orientation of  $\sigma_1$  seems to be generally deflected into a N–S to NNE–SSW direction. This deflection is possibly caused by structural inheritance of pre-existing discontinuities such as the normal faults typical for this area. In the Deformed Tabular Jura and the Folded Jura, the questionable NNE–SSW to NE–SW trending shortening directions are often found to be perpendicular to major compression related structures (e.g. locations 14, 35 in Fig. 12). In these cases, NNE–SSW to NE–SW shortening is interpreted to reflect local stress/strain field perturbations known to occur in the vicinity of major fault zones (e.g. Homberg et al. 1997). In summary, both observed shortening directions are considered to be related to the same Late Miocene regional stress field characterized by  $\sigma_1$  trending roughly NNW–SSE. This interpretation is in line with the results of previous studies in the central part of the Jura Fold-and-Thrust Belt that also revealed a very complex shortening pattern associated with the formation of the range (e.g. Homberg et al. 2002).

### 5.6 Post-Jura folding and recent fracture sets?

Occasionally, strike-slip faults were found to postdate folding of the sedimentary stack related to the thin-skinned formation of the Jura Fold-and-Thrust Belt (Fig. 10). With very few exceptions (compare Fig. 15), the shortening directions derived from the kinematic analysis of pre- and post-folding fracture sets do not significantly deviate from

each other (e.g. locations 1, 4, 42 in Fig. 13);  $\sigma_1$  consistently strikes NNW–SSE. No distinctive fracture sets or shortening directions related to anything different than thin-skinned formation of the Jura Fold-and-Thrust Belt, for example a younger thick-skinned tectonic stage (compare Sect. 2), can be distinguished. In fact, the present-day stress field as constrained by a compilation of several different indicators (Reinecker et al. 2010) very much mimics the one reconstructed during this study. It appears that this stress field had already initiated in northern Switzerland in Late Miocene times, prior to the comparatively late formation of the Jura Fold-and-Thrust Belt, and has not significantly changed since then.

## 6 Conclusions

The summary of the results of an extensive analysis of outcrop-scale brittle deformation structures across central northern Switzerland allows an enhanced structural geological characterization of the region. Of particular interest is the extent to which it was affected by various regionally recognized Cenozoic tectonic events at outcrop scale.

Characteristic outcrop-scale brittle deformation features in the study area are bedding-orthogonal joints. In the studied outcrops of Jurassic limestone, the spacing of these fractures is often very close (less than 1 meter). Faults showing measurable offsets (e.g. >several millimeters) are observed comparatively rarely and are apparently restricted to locations in the vicinity of map-scale fault zones.

The systematic analysis of outcrop-scale fractures allowed a relative chronology of Cenozoic brittle deformation to be established and a regional fault-slip analysis to be performed. In general, reactivation of pre-existing fractures is a very commonly observed phenomenon. In particular, the regionally recognized, bedding-orthogonal joints were repeatedly reactivated during later tectonic events. Locally, the fracture patterns and deformation sequences are more complex due to the influence of regional fault zones.

On the scale of the study area, three Cenozoic deformation events had a significant imprint on the outcrop-scale fracture patterns: (1) formation of bedding-orthogonal joints most likely related to regional uplift in Latest Mesozoic to Paleogene times; (2) a locally recognized, close to radial extension phase in the vicinity of the Hegau-Lake Constance Graben, with  $\sigma_3$  oriented NE–SW and NW–SE, which started after the Early Miocene; (3) shortening of the Alpine foreland from the Late Miocene onwards. Regionally recognized NW–SE to NNW–SSE shortening, manifested by the strike-slip reactivation of bedding-orthogonal joints as well as locally developed reverse faults, already initiated prior to

the formation of folding and thrusting in the Eastern Jura Mountains, but continued to be active throughout this deformation event. Only locally recognizable NNE–SSW to NE–SW directed shortening directions are interpreted in the same tectonic context and most likely represent local perturbations of the associated regional strain/stress field due to the commonly observed reactivation of pre-existing fracture networks and the influence of regional fault zones.

At the outcrop scale, it appears that some important tectonic events in the surroundings of the study area, such as the opening of the Upper Rhine Graben further to the west, had hardly any recognizable tectonic imprint. Other events such as the uplift of the Black Forest, the subsidence of the Molasse Basin and the formation of the Hegau-Lake Constance Graben apparently only had a very local effect on the outcrop-scale fracture systems since restricted to sites in the vicinity of reactivated basement faults.

Late Miocene NNW–SSE oriented shortening directions derived from the kinematic analysis of outcrop-scale fractures and the orientation of maximum horizontal stress given by various recent stress indicators are roughly parallel to each other. This observation suggests that the regional stress field may not have changed significantly across the study area since the Late Miocene.

**Acknowledgments** This article is based on a field study carried out by Nagra. P. Hammer is thanked for his assistance in the field and his support in the preparation of the associated Nagra working report (note that this Nagra report as well as all others cited herein can be downloaded directly from the Nagra homepage or received from the Nagra Infocenter upon request; refer to <http://www.nagra.ch>). The constructive manuscript reviews by J. Mosar, M. Meschede, J.G. Ramsay and the associated editor S.M. Schmid are kindly acknowledged. I would like to dedicate this publication to the memory of the late Peter Blümling who was a pioneer in the investigation of crustal stresses in Western Europe and whose initiative and trust allowed me to carry out this exhilarating field project.

## References

- Allenbach, R. P. (2001). Synsedimentary tectonics in an epicontinental sea: a new interpretation of the Oxfordian basins of northern Switzerland. *Eclogae Geologicae Helveticae*, 94(3), 265–287.
- Anderson, E. M. (1942). *The Dynamics of Faulting and Dyke Formation with Applications to Britain* (pp. 206), Edinburgh: Oliver and Boyd.
- Angelier, J. (1989). From orientation to magnitudes in paleostress determinations using fault slip data. *Journal of Structural Geology*, 11, 37–50.
- Angelier, J. (1990). Inversion of field data in fault tectonics to obtain the regional stress. III. A new rapid direct inversion method by analytical means. *Geophysical Journal International*, 103, 363–376.
- Angelier, J., & Mechler, P. (1977). Sur une méthode graphique de recherche des contraintes principales également utilisable en

- tectonique et en séismologie: la méthode des dièdres droits. *Bulletin de la Société géologique de France*, 19, 1309–1318.
- Becker, A. (2000). The Jura Mountains—an active foreland fold-and-thrust belt? *Tectonophysics*, 321, 381–406.
- Bergerat, F. (1987). Stress fields in the European Platform at the time of Africa-Eurasia collision. *Tectonics*, 6(2), 99–132.
- Bott, M. (1959). The mechanics of oblique slip faulting. *Geological Magazine*, 96, 109–117.
- Burkhard, M. (1990). Aspects of the large-scale Miocene deformation in the most external part of the Swiss Alps (Subalpine Molasse to Jura fold belt). *Eclogae Geologicae Helveticae*, 83, 559–583.
- Buxtorf, A. (1907). Zur Tektonik des Kettenjura. *Berichte über die Versammlungen des Oberrheinischen Geologischen Vereins*, 40, 29–38.
- Célérier, B., Etchecopar, A., Bergerat, F., Vergely, P., Arthaud, F., & Laurent, P. (2012). Inferring stress from faulting: from early concepts to inverse methods. *Tectonophysics*, 581, 206–2019.
- Dèzes, P., Schmid, S. M., & Ziegler, P. A. (2004). Evolution of the European Cenozoic Rift System. Interaction of the Alpine and Pyrenean orogens with their foreland lithosphere. *Tectonophysics*, 389, 1–33.
- Diebold, P., Naef, H., Ammann, M. (1991). *Zur Tektonik der zentralen Nordschweiz. Interpretation aufgrund regionaler Seismik, Oberflächengeologie und Tiefbohrungen*. Nagra Technical Report NTB 90-04 (pp. 277). Wettingen: Nagra.
- Diebold, P., & Noack, T. (1997). Late Paleozoic troughs and Tertiary structures in the eastern folded Jura. In P. Heitzmann & P. Lehner (Eds.), *Deep structure of the Swiss Alps*. Basel: Birkhäuser Verlag.
- Geyer, M., Nitsch, E., Simon, T. (2011). *Geologie von Baden-Württemberg* (pp. 627). Stuttgart: Schweizerbart.
- Giamboni, M., Ustaszewski, K., Schmid, S. M., Schumacher, M. E., & Wetzler, A. (2004). Plio-Pleistocene transpressional reactivation of Paleozoic and Paleogene structures in the Rhine-Bresse Transform Zone (northern Switzerland and eastern France). *International Journal of Earth Sciences*, 93, 207–223.
- Gygi, R. A. (1986). Eustatic sea level changes of the Oxfordian (Late Jurassic) and their effect documented in sediments and fossil assemblages of an epicontinental sea. *Eclogae Geologicae Helveticae*, 79(2), 455–491.
- Hancock, P. L. (1985). Brittle microtectonics: principles and practice. *Journal of Structural Geology*, 7, 437–457.
- Hergert, T., Heidebach, O., Reiter, K., Giger, S., & Marschall, P. (2015). Stress field sensitivity analysis in a sedimentary sequence of the Alpine foreland, Northern Switzerland. *Solid Earth*, 6, 711–756.
- Hindle, D., & Burkhard, M. (1999). Strain, displacement and rotation associated with the formation of curvature in fold belts; the example of the Jura arc. *Journal of Structural Geology*, 21(8-9), 1089–1101.
- Hinsken, S., Ustaszewski, K., & Wetzler, A. (2007). Graben width controlling syn-rift sedimentation. The Palaeogene southern Upper Rhine Graben as an example. *International Journal of Earth Sciences*, 96, 979–1002.
- Hippolyte, J.-C., Bergerat, F., Gordon, M. B., Bellier, O., & Espurt, N. (2012). Keys and pitfalls in mesoscale fault analysis and paleostress reconstructions, the use of Angelier's methods. *Tectonophysics*, . doi:10.1016/j.tecto.2012.01.012.
- Hoepfener, R. (1955). Tektonik im Schiefergebirge; eine Einführung. *Geologische Rundschau*, 44, 26–58.
- Hofmann, F. and Hantke, R. (1964). *Geological Atlas Switzerland 1:25'000: Map sheet 1032 Diessenhofen, Annotations* (pp. 45). Wabern: Swisstopo.
- Hofmann, F., Schlatter, R., Weh, M. (2000). *Geological Atlas of Switzerland 1:25'000: Map sheets 1011/1012 Beggingen/Singen, Annotations* (pp. 113). Wabern: Swisstopo.
- Homberg, C., Bergerat, F., Philippe, Y., Lacombe, O., & Angelier, J. (2002). Structural inheritance and Cenozoic stress fields in the Jura fold-and-thrust belt (France). *Tectonophysics*, 357, 137–158.
- Homberg, C., Hu, J., Angelier, J., Bergerat, F., & Lacombe, O. (1997). Characterization of stress perturbations near major fault zones: insights from field studies (Jura Mountains) and numerical modelling. *Journal of Structural Geology*, 19(5), 703–718.
- Homberg, C., Lacombe, O. J., Angelier, J., & Bergerat, F. (1999). New constraints for indentation mechanisms in arcuate belts from the Jura Mountains, France. *Geology*, 27, 827–830.
- Ibele, T. (2015). *Tectonics of the Hegau and Lake Constance region: a synthesis based on existing literature*. Nagra working report NAB 12–23 (pp. 57). Wettingen: Nagra.
- Illies, J. H. (1981). Mechanism of Graben formation. *Tectonophysics*, 73, 249–266.
- Jordan, P. (1992). Evidence for large-scale decoupling in the Triassic evaporites of northern Switzerland: an overview. *Eclogae Geologicae Helveticae*, 85(677), 693.
- Jordan, P., Noack, T., Widmer, T. (1990). The evaporite shear zone of the Jura Boundary Thrust; new evidence from Wisen Well (Switzerland). In: P. Jordan, T. Noack, S. Schmid, D. Bernoulli (Eds.): *The Hans Laubscher volume. Eclogae Geologicae Helveticae 83/3* (pp. 25–542). Basel: Birkhäuser Verlag.
- Kastrup, U., Zoback, M.-L., Deichmann, N., Evans, K., Giardini, D., & Michael, A. J. (2004). Stress field variations in the Swiss Alps and the northern Alpine foreland derived from inversion of fault plane solutions. *Journal of Geophysical Research*, 109, B01402. doi:10.1029/2003JB002550.
- Kaven, J. O., Maerten, M., & Pollard, D. D. (2011). Mechanical analysis of fault slip data: implications for paleostress analysis. *Journal of Structural Geology*, 33(2), 78–91.
- Kempf, O., & Pfiffner, O. A. (2004). Early Tertiary evolution of the North Alpine Foreland Basin of the Swiss Alps and adjoining areas. *Basin Research*, 16, 549–567.
- Lacombe, O. (2012). Do fault slip data inversions actually yield “paleostresses” that can be compared with contemporary stresses? A critical discussion. *Comptes Rendus Geo-science*, 344, 159–173.
- Larroque, J., & Laurent, P. (1988). Evolution of the stress field pattern in the south of the Rhine Graben from the Eocene to the present. *Tectonophysics*, 148, 41–58.
- Laubscher, H. (1970). Grundsätzliches zur Tektonik des Rheingrabens. In J. H. Illies, S. Mueller. (Eds.), *Graben Problems. Proceedings of an International Rift Symposium held in Karlsruhe 1968, International Upper Mantle Project* (pp. 79-86). Stuttgart: E. Schweizerbart'sche.
- Laubscher, H. (1972). Some overall aspects of Jura dynamics. *American Journal of Science*, 272, 293–304.
- Laubscher, H. (1986). The eastern Jura: relations between thin-skinned and basement tectonics, local and regional. *Geologische Rundschau*, 75, 535–553. doi:10.1007/BF01820630.
- Madritsch, H., Hammer, P. (2012). *Characterisation of Cenozoic brittle deformation of potential geological siting regions for radioactive waste repositories in Northern Switzerland based on structural geological analysis of field outcrops*. Nagra working report NAB 12–41 (pp. 163). Wettingen: Nagra.
- Madritsch, H., Kounov, A., Schmid, S. M., & Fabbri, O. (2009). Multiple fault reactivations within the intracontinental Rhine-Bresse Transfer Zone (La Serre Horst, eastern France). *Tectonophysics*, 471, 297–318.
- Madritsch, H., Preusser, F., Fabbri, O., Bichet, V., Schlunegger, F., & Schmid, S. M. (2010). Late Quaternary folding in the Jura Mountains: evidence from syn-erosional deformation of fluvial meanders. *Terra Nova*, 22, 147–154.
- Madritsch, H., Schmid, S.M., Fabbri, O. (2008). Interactions between thin- and thick-skinned tectonics at the northwestern front of the

- Jura fold-and-thrust-belt (eastern France). *Tectonics* 27, TC5005, doi:10.1029/2008TC002282.
- Malz, A., Madritsch, H., Kley, J. (2015). Improving 2D-reflection seismic interpretation in challenging settings by integration of restoration techniques: A case study from the Jura fold-and-thrust-belt (Switzerland). *Interpretation* 3/4, SAA37–SAA58. doi:10.1190/INT-2015-0012.1.
- Mandl, G. (2005). *Rock Joints. The mechanical genesis* (pp. 222). Berlin: Springer.
- Marrett, R., & Allmendinger, R. W. (1990). Kinematic analysis of fault-slip data. *Journal of Structural Geology*, 12, 973–986. doi:10.1016/0191-8141(90)90093-E.
- Marrett, R., & Peacock, D. C. P. (1999). Strain and stress. *Journal of Structural Geology*, 21, 1061–1067.
- Mazurek, M., Hurford, A. J., & Leu, W. (2006). Unravelling the multi-stage burial history of the Swiss Molasse Basin: integration of apatite fission track, vitrinite reflectance and biomarker isomerisation analysis. *Basin Research*, 18, 27–50.
- Meier, D. (1984). Zur Tektonik des schweizerischen Tafel- und Faltenjura (regionale und lokale Strukturen, Kluftgenese, Bruch und Falten tektonik, Drucklösung). *Ph.D. dissertation*, Universität Clausthal, Clausthal Zellerfeld, Germany, pp. 75.
- Meier, D., & Kronberg, P. (1989). *Klüftung in Sedimentgesteinen* (p. 116). Stuttgart: Ferdinand Enke.
- Meschede, M. (1994). *Methoden der Strukturgeologie (169 pp)*. Stuttgart: Ferdinand Enke.
- Meschede, M., & Decker, K. (1993). Störungsflächenanalyse entlang des Nordrandes der Ostalpen—Ein methodischer Vergleich. *Z. Dtsch. Geol. Ges.*, 144, 419–433.
- Mosar, J. (1999). Present-day and future tectonic underplating in the western Swiss Alps: reconciliation of basement/wrench-faulting and décollement folding of the Jura and Molasse basin in the Alpine foreland. *Earth and Planetary Science Letters*, 173, 143–155.
- Müller, W.H., Naef, H., Graf, H.R. (2002). *Geologische Entwicklung der Nordschweiz, Neotektonik und Langzeitszenarien im Zürcher Weinland. Nagra Technical Report NTB 99-08* (pp. 237), Wettingen: Nagra.
- Naef, H., Birkhäuser, P., Roth, P. (1995). *Interpretation der Reflexionsseismik im Gebiet Nördlich Lägern—Zürcher Weinland. Nagra Technical Report NTB 94-14* (120 pp). Wettingen: Nagra.
- Nagra (2014). *SGT-Etappe 2: Vorschlag weiter zu untersuchender geologischer Standortgebiete mit zugehörigen Standortarealen für die Oberflächenanlagen: Geologische Grundlagen, Sedimentologische und tektonische Verhältnisse*. Nagra Technical Report NTB 14-02, Dossier II (pp. 237). Wettingen: Nagra.
- Nivière, B., & Winter, T. (2000). Pleistocene northwards fold propagation of the Jura within the southern Upper Rhine Graben: seismotectonic implications. *Global and Planetary Change*, 27, 263–288.
- Ortner, H., Reiter, F., & Acs, P. (2002). Easy handling of tectonic data: the programs TectonicVB for Mac and Tectonics FP for Windows™. *Computers and Geosciences*, 28(10), 1193–1200.
- Petit, J. P. (1987). Criteria for the sense of movement on fault surfaces in brittle rocks. *Journal of Structural Geology*, 9(5-6), 597–608.
- Pfiffner, O. A. (1986). Evolution of the north Alpine foreland basin in the Central Alps. In P. A. Allen, P. Homewood P. (Eds.), *Foreland Basins. Int. Assoc. Sediment. Spec. Publ.* 8 (pp. 219–228).
- Pfiffner, O. A., & Burkhard, M. (1987). Determination of paleo-stress axes orientations from fault, twin and earthquake data. *Annales Tectonicae*, 1, 48–57.
- Plessmann, W. (1972). Horizontal-Sylolithen im französisch-schweizerischen Tafel- und Faltenjura und ihre Einpassung in den regionalen Rahmen. *Geologische Rundschau*, 61, 332–347.
- Pollard, D. D., Saltzer, S. D., & Rubin, A. M. (1993). Stress inversion methods: are they based on faulty assumption? *Journal of Structural Geology*, 15, 1045–1054. doi:10.1016/0191-8141(93)90176-B.
- Rahn, M., & Selbekk, R. (2007). Absolute dating of the youngest sediments of the Swiss Molasse basin by apatite fission track analyses. *Swiss Journal of Geosciences*, 100(3), 371–381.
- Ramsay, J.G., Huber, M.I. (1987). *The techniques of modern structural geology. Volume 2: Folds and Fractures* (pp. 700). London: Academic press.
- Reicherter, K., Froitzheim, N., Jarosinski, M., Badura, J., Franzke, H.-J., Hansen, M., et al. (2008). Alpine tectonics north of the Alps. In T. McCann (Ed.), *The geology of Central Europe* (pp. 1233–1285). London: The Geological Society.
- Reinecker, J., Tingay, M., Müller, B., & Heidbach, O. (2010). Present-day stress orientation in the Molasse Basin. *Tectonophysics*, 482, 129–138.
- Rittner, M. (2013). U-Pb dating of brittle deformation. *Unpubl. Ph.D. Dissertation*, Royal Holloway University London, London, UK, pp. 270.
- Schlunegger, F., Jordan, T. E., & Klaper, E. M. (1997). Controls of erosional denudation in the orogen on foreland basin evolution: the Oligocene central Swiss Molasse Basin as an example. *Tectonics*, 16, 823–840.
- Schmid, S. M., Pfiffner, O. A., Froitzheim, N., Schönborn, G., & Kissling, E. (1996). Geophysical-geological transect and tectonic evolution of the Swiss-Italian Alps. *Tectonics*, 15, 1036–1064.
- Schmid, S. M., Pfiffner, O. A., Schönborn, G., Froitzheim, N., & Kissling, E. (1997). Integrated cross section and tectonic evolution of the Alps along the Eastern Traverse. In O. A. Pfiffner, P. Lehner, P. Heitzman, & S. Müller (Eds.), *Deep structure of the Swiss Alps: Results of NRP 20* (pp. 289–304). Basel: Birkhäuser Verlag.
- Schreiner, A. (1992). *Geological Map of Baden-Württemberg 1:50 000: Hegau und westlicher Bodensee, Annotations* (p. 290). Freiburg: LGRB.
- Schumacher, M.E. (2002). Upper Rhine Graben: role of preexisting structures during rift evolution. *Tectonics* 21/1, 6-1–6-17.
- Sinclair, H., & Allen, P. A. (1992). Vertical versus horizontal motions in the Alpine orogenic wedge: stratigraphic response in the Foreland Basin. *Basin Research*, 4, 215–232.
- Sippel, J., Scheck-Wenderoth, M., Reicherter, K., & Mazur, S. (2009). Paleostress states at the southwestern margin of the Central European Basin System—application of fault-slip analysis to unravel a polyphase deformation pattern. *Tectonophysics*, 470(1-2), 129–146.
- Sommaruga, A. (1997). *Geology of the central Jura and the Molasse Basin: new insight into an evaporite-based foreland fold and thrust belt* (p. 176). Neuchâtel: Mém. Soc. neuchâtel. Sci. nat., T. XII.
- Sperner, B., & Zweigel, P. (2010). A plea for more caution in fault-slip analysis. *Tectonophysics*, 482, 29–41.
- Thury, M., Gautschi, A., Mazurek, M., Müller, W. H., Naef, H., Pearson, F. J., Vomvoris, S., Wilson, W. (1994). *Geology and hydrogeology of the crystalline basement of Northern Switzerland. Nagra Technical Report NTB 93-01* (pp. 464). Wettingen: Nagra.
- Timar-Geng, Z., Fügenschuh, B., Wetzel, A., & Dresmann, H. (2006). The low temperature thermal history of northern Switzerland as revealed by fission track analysis and inverse thermal modelling. *Eclogae Geologicae Helveticae*, 99, 255–270.
- Turner, F. J. (1953). Nature and dynamic interpretation of deformation lamellae in calcite of three marbles. *American Journal of Science*, 251, 276–298.
- Twiss, R. J., & Unruh, J. R. (1998). Analysis of fault slip inversions: do they constrain stress or strain rate? *Journal Geophysical Research*, 103(12), 205–222. doi:10.1029/98JB00612.

- Ustaszewski, K., & Schmid, S. M. (2007). Latest Pliocene to recent thick-skinned tectonics at the Upper Rhine Graben—Jura Mountains junction. *Swiss Journal of Geosciences*, 100(2), 293–312.
- Ustaszewski, K., Schumacher, M. E., & Schmid, S. M. (2005). Simultaneous normal faulting and extensional flexuring during rifting—an example from the southernmost Upper Rhine Graben. *International Journal of Earth Sciences*, 94, 680–696.
- Wallace, R. E. (1951). Geometry of shearing stress and relation to faulting. *Journal of Geology*, 59, 118–130.
- Wetzel, A., Allenbach, R., & Allia, V. (2003). Reactivated basement structures affecting the sedimentary facies in a tectonically “quiescent” epicontinental basin: an example from NW Switzerland. *Sedimentary Geology*, 157, 153–172.
- Wildi, W. (1975). Die Mettauer Überschiebung im Aargauischen Tafeljura (Nordschweiz). *Eclogae Geologicae Helvetiae*, 68(3), 483–489.
- Willet, S. D., & Schlunegger, F. (2010). The last phase of deposition in the Swiss Molasse Basin: from foredeep to negative-alpha basin. *Basin Research*, 22, 623–639.
- Ziegler, P. A. (1992). European Cenozoic Rift System. *Tectonophysics*, 208, 91–111.
- Ziegler, P. A., & Fraefel, M. (2009). Response of drainage systems to Neogene evolution of Jura fold-thrust belt and Upper Rhine Graben. *Swiss Journal of Geosciences*, 102, 57–75.